sheep recombinant PrPs in mice might be attributable to these different amino acids. About half of these different amino acids in bovine and sheep PrPs are concentrated in the regions corresponding to moPrP90–109, moPrP131–154, and moPrP219–231. Bovine and sheep PrPs possess 2 and 3, 4 and 3, and 4 and 4 different amino acids in the corresponding moPrP90–109, moPrP131–154, and moPrP219–231 regions, respectively. It is therefore possible that these regions of bovine and sheep PrPs are immunogenic in mice because of the different amino acid composition, eliciting antibodies, which were not only specific to themselves but also to the corresponding mouse epitopes. In other words, heterologous bovine and sheep PrPs might mimic host mouse PrP to overcome tolerance. Taken together, our present results might open a new avenue for development of molecular mimicry-based prion vaccines.

Acknowledgments

We all thank Prof. Motohiro Horiuchi (Hokkaido University) for providing a cloned bovine PrP cDNA and a cloned sheep genomic PrP DNAs. This study is partly supported by a Research on Specific Diseases from the Ministry of Health, Labour and Welfare, Japan.

References

[1] Prusiner SB. Prions. Proc Natl Acad Sci USA 1998;95(23):13363–83.
[2] Weissmann C, Enari M, Klohn PC, Rossi D, Flechsig E. Molecular biology of prions. Acta Neurobiol Exp (Wars) 2002;62(3):153–66.
[3] Wilesmith JW, Wells GA, Cranwell MP, Ryan JB. Bovine spongiform encephalopathy: epidemiological studies. Vet Rec 1988; 123(25):638–44.
[4] Hill AF, Desbruslais M, Joiner S, et al. The same prion strain causes vCJD and BSE. Nature 1997;389(6650), 448–50, 526.
[5] Bruce ME, Will RG, Ironside JW, et al. Transmissions to mice indicate that 'new variant' CJD is caused by the BSE agent. Nature 1997;389(6650):498–501.
[6] Llewelyn CA, Hewitt PE, Knight RSG, et al. Possible transmission of variant Creutzfeldt–Jakob disease by blood transfusion. Lancet 2004;363:417–21.
[7] Peden AH, Head MW, Ritchie DL, Bell JE, Ironside JW. Preclinical vCJD after blood transfusion in a PRNP codon 129 heterozygous patient. Lancet 2004;364:527–9.
[8] Gabizon R, McKinley MP, Groth D, Prusiner SB. Immunoaffinity purification and neutralization of scrapie prion infectivity. Proc Natl Acad Sci USA 1988;85(18):6617–21.
[9] Heppner FL, Musahl C, Arrighi I, et al. Prevention of scrapie pathogenesis by transgenic expression of anti-prion protein antibodies. Science 2001;294(5540):178–82.
[10] White AR, Enever P, Tayebi M, et al. Monoclonal antibodies inhibit prion replication and delay the development of prion disease. Nature 2003;422(6927):80–3.
[11] Tateishi J, Ohta M, Koga M, Sato Y, Kuroiwa Y. Transmission of chronic spongiform encephalopathy with kuru plaques from humans to small rodents. Ann Neurol 1979;5(6):581–4.
[12] Peretz D, Williamson RA, Kaneko K, et al. Antibodies inhibit prion propagation and clear cell cultures of prion infectivity. Nature 2001;412(6848):739–43.
[13] Sigurdsson EM, Brown DR, Daniels M, et al. Immunization delays the onset of prion disease in mice. Am J Pathol 2002;161(1):13–7.
[14] Bainbridge J, Walker B. Cell mediated immune responses against human prion protein. Clin Exp Immunol 2003;133(3):310–7.
[15] Mabbott NA, Bruce ME, Botto M, Walport MJ, Pepys MB. Temporary depletion of complement component C3 or genetic deficiency of C1q significantly delays onset of scrapie. Nat Med 2001;7(4):485–7.
[16] Klein MA, Kaeser PS, Schwarz P, et al. Complement facilitates early prion pathogenesis. Nat Med 2001;7(4):488–92.
[17] Polymenidou M, Heppner FL, Pellicioli EC, et al. Humoral immune response to native eukaryotic prion protein correlates with anti-prion protection. Proc Natl Acad Sci USA 2004;101:14670–6.
[18] Gilch S, Wopfner F, Renner-Muller I, et al. Polyclonal anti-PrP auto-antibodies induced with dimeric PrP interfere efficiently with PrPSc propagation in prion-infected cells. J Biol Chem 2003;278(20):18524–31.
[19] Behar SM, Porcelli SA. Mechanisms of autoimmune disease induction. The role of the immune response to microbial pathogens. Arthritis Rheum 1995;38(4):458–76.
[20] Ang CW, Jacobs BC, Laman JD. The Guillain–Barre syndrome: a true case of molecular mimicry. Trends Immunol 2004;25(2):61–6.
[21] Schatzl HM, Da Costa M, Taylor L, Cohen FE, Prusiner SB. Prion protein gene variation among primates. J Mol Biol 1997;265(2): 257.
[22] Donne DG, Viles JH, Groth D, et al. Structure of the recombinant full-length hamster prion protein PrP(29–231): the N terminus is highly flexible. Proc Natl Acad Sci USA 1997;94(25):13452–7.
[23] Riek R, Hornemann S, Wider G, Glockshuber R, Wuthrich K. NMR characterization of the full-length recombinant murine prion protein, mPrP(23–231). FEBS Lett 1997;413(2):282–8.

Available online at www.sciencedirect.com
ScienceDirect
Gene 386 (2007) 139–146
GENE
SECTION
FUNCTIONAL GENOMICS
www.elsevier.com/locate/gene

Newly established *in vitro* system with fluorescent proteins shows that abnormal expression of downstream prion protein-like protein in mice is probably due to functional disconnection between splicing and 3′ formation of prion protein pre-mRNA

Daisuke Yoshikawa [a], Juraj Kopacek [a,b], Naohiro Yamaguchi [a], Daisuke Ishibashi [c], Hitoki Yamanaka [c], Yoshitaka Yamaguchi [c], Shigeru Katamine [a], Suehiro Sakaguchi [a,c,d,*]

[a] *Department of Molecular Microbiology and Immunology, Nagasaki University Graduate School of Biomedical Sciences, Sakamoto 1-12-4, Nagasaki 852-8523, Japan*
[b] *Department of Molecular Biology, Institute of Virology, Slovak Academy of Sciences, Bratislava, Slovakia*
[c] *PRESTO Japan Science and Technology Agency, 4-1-8 Honcho Kawaguchi, Saitama, Japan*
[d] *Division of Molecular Cytology, Institute for Enzyme Research, The University of Tokushima, 3-18-15 Kuramoto-cho, Tokushima 770-8503, Japan*

Received 10 July 2006; received in revised form 8 August 2006; accepted 25 August 2006
Available online 15 September 2006
Received by A. Bernardi

Abstract

We and others previously showed that, in some lines of prion protein (PrP)-knockout mice, the downstream PrP-like protein (PrPLP/Dpl) was abnormally expressed in brains partly due to impaired cleavage/polyadenylation of the residual PrP promoter-driven pre-mRNA despite the presence of a poly(A) signal. In this study, we newly established an *in vitro* transient transfection system in which abnormal expression of PrPLP/Dpl can be visualized by expression of the green fluorescence protein, EGFP, in cultured cells. No EGFP was detected in cells transfected by a vector carrying a PrP genomic fragment including the region targeted in the knockout mice intact upstream of the PrPLP/Dpl gene. In contrast, deletion of the targeted region from the vector caused expression of EGFP. By employing this system with other vectors carrying various deletions or point mutations in the targeted region, we identified that disruption of the splicing elements in the PrP terminal intron caused the expression of EGFP. Recent lines of evidence indicate that terminal intron splicing and cleavage/polyadenylation of pre-mRNA are functionally linked to each other. Taken together, our newly established system shows that the abnormal expression of PrPLP/Dpl in PrP-knockout mice caused by the impaired cleavage/polyadenylation of the PrP promoter-driven pre-mRNA is due to the functional dissociation between the pre-mRNA machineries, in particular those of cleavage/polyadenylation and splicing. Our newly established *in vitro* system, in which the functional dissociation between the pre-mRNA machineries can be visualized by EGFP green fluorescence, may be useful for studies of the functional connection of pre-mRNA machineries.

Keywords: Intergenic splicing; *In vitro* system; Purkinje cell degeneration; Fluorescent protein

1. Introduction

Prnd is a recently identified gene encoding the first prion protein (PrP)-like protein, PrPLP/Doppel (Dpl), locating 16-kb downstream of the PrP gene, *Prnp* (Moore et al., 1999; Li et al., 2000a). *Prnd* is actively expressed in the testis, heart, skeletal muscle, and spleen, but not in the brain, whereas *Prnp* is the most abundantly expressed in the brain (Li et al., 2000b). Male mice devoid of PrPLP/Dpl were shown to be infertile due to

Abbreviations: PrP, prion protein; PrPLP/Dpl, PrP-like protein/Doppel; bp, base pair; PCR, polymerase chain reaction; nt, nucleotides; EGFP, enhanced green fluorescence protein; UTR, untranslated region; ORF, open reading frame; DMEM, Dulbecco's Modified Eagle Medium; RACE, rapid amplification of cDNA ends; HCMV, human cytomegalovirus; RNP, ribonucleoprotein; PAP, poly(A) polymerase; CPSF, cleavage/polyadenylation specificity factor.

* Corresponding author. Division of Molecular Cytology, Institute for Enzyme Research, The University of Tokushima, 3-18-15 Kuramoto-cho, Tokushima 770-8503, Japan. Tel.: +81 88 633 7438; fax: +81 88 633 7440.
E-mail address: sakaguch@ier.tokushima-u.ac.jp (S. Sakaguchi).

0378-1119/$ - see front matter © 2006 Elsevier B.V. All rights reserved.
doi:10.1016/j.gene.2006.08.028

abnormal development of sperm, indicating that PrPLP/Dpl is important for spermatogenesis (Behrens et al., 2002).

We and others found that PrPLP/Dpl is toxic when ectopically expressed in neurons deficient for the cellular PrP (PrP^C) (Moore et al., 2001; Anderson et al., 2004; Yamaguchi et al., 2004). Some lines of mice devoid of PrP^C ($Prnp^{0/0}$), including Ngsk $Prnp^{0/0}$, Rcm0 $Prnp^{0/0}$, and Zrch II $Prnp^{0/0}$, developed ataxia and Purkinje cell degeneration due to the ectopic expression of PrPLP/Dpl in neurons, but others, such as Zrch I $Prnp^{0/0}$ and Npu $Prnp^{0/0}$, showed neither the ectopic expression of PrPLP/Dpl nor such neurological abnormalities (Bueler et al., 1992; Manson et al., 1994; Sakaguchi et al., 1996; Moore et al., 1999; Rossi et al., 2001). In the ataxic lines of $Prnp^{0/0}$ mice, *Prnd* was aberrantly regulated under the control of *Prnp* promoter and thereby ectopically expressed in the brain, especially in neurons, where the *Prnp* promoter is very active (Moore et al., 1999; Li et al., 2000a). The ectopically expressing PrPLP/Dpl mRNAs were chimeric, comprising the residual *Prnp* non-coding exons 1 and 2 at the 5′ end followed by the *Prnd*-coding exons, due to an abnormal intergenic splicing taking place between *Prnp* and *Prnd* (Moore et al., 1999; Li et al., 2000a). The mechanism of how *Prnd* became abnormally regulated under the control of the *Prnp* promoter in the ataxic lines of $Prnp^{0/0}$ mice remains to be studied.

In wild-type mice, PrP pre-mRNA is normally cleaved and polyadenylated at the end of *Prnp*. However, in ataxic lines of $Prnp^{0/0}$ mice, the pre-mRNA was unsuccessfully cleaved and polyadenylated at the end of *Prnp*, resulting in its elongation until the end of downstream *Prnd* (Moore et al., 1999; Li et al., 2000a), indicating that the abnormal regulation of *Prnd* in these mice could be in part attributable to the impaired cleavage/polyadenylation of *Prnp* pre-mRNA. A polyadenylation signal is essential for the pre-mRNA cleavage/polyadenylation processes. However, the polyadenylation signal of *Prnp* and its flanking sequences are intact in two ataxic lines of Ngsk $Prnp^{0/0}$ and Rcm0 $Prnp^{0/0}$ mice. It is recently believed that the pre-mRNA processes, including acquisition of a cap structure at the 5′ end, splicing out of introns, and cleavage/polyadenylation at the 3′ end, are functionally linked to each other during transcription (Steinmetz, 1997; Proudfoot et al., 2002; Kornblihtt et al., 2004). In particular, the cleavage/polyadenylation processes are strongly influenced by splicing of the terminal intron. In the ataxic lines of $Prnp^{0/0}$ mice, a part of the *Prnp* terminal intron including the elements important for splicing, such as a splice branch point, a polypyrimidine tract, and a splice acceptor, is commonly targeted as well as the subsequent half of the last exon (Sakaguchi et al., 1995; Moore et al., 1999; Rossi et al., 2001). Thus, disruption of these splicing elements due to deletion of intron 2 could cause functional dissociation between splicing and cleavage/polyadenylation for the *Prnp* pre-mRNA in the ataxic lines of $Prnp^{0/0}$ mice, resulting in the impaired cleavage/polyadenylation of the pre-mRNA. It is alternatively possible that deletion of the exonic sequences in *Prnp* might disturb the cleavage/polyadenylation processes for the *Prnp* pre-mRNA.

In the present study, we established an *in vitro* transient transfection system in which abnormal expression of PrPLP/Dpl can be visualized by expression of the green fluorescence protein, EGFP, in cultured cells. Using this system, we identified that the abnormal expression of PrPLP/Dpl could be attributed to the functional disconnection between splicing and cleavage/polyadenylation processes. These results indicate usefulness of our newly established *in vitro* system for studying the functional connection of pre-mRNA machineries because the functional dissociation between the pre-mRNA machineries can be easily visualized by EGFP green fluorescence.

2. Materials and methods

2.1. Expression vectors

2.1.1. pPrPwild

The 488- and 2688-bp genomic fragments of *Prnd*, spanning nucleotides (nt) 35,716 to 36,204 (GenBank accession no. *U29187*) and nt 36,712 to 39,400, respectively, were first amplified from mouse genomic DNA using polymerase chain reaction (PCR; Advantage cDNA PCR KIT, Clontech, California, USA) with appropriate sets of a primer pair. The former, corresponding to a part of intron 1 and an entire 5′ untranslated region (UTR) of *Prnd*, possessed the *Sal* I and *Nhe* I enzyme sites at the 5′ and 3′ ends, respectively. The latter, consisting of an entire 3′ UTR and the downstream intervening sequence, had the *Bam*H I and *Mlu* I sites at its 5′ and 3′ ends, respectively. These fragments were ligated with the enhanced green fluorescence protein (EGFP)-coding *Nhe* I–*Bam*H I insert of pEGFP-C1 (Clontech) in such a way that the EGFP insert was flanked by the genomic fragments, and cloned into the *Sal* I and *Mlu* I sites of a pDON-AI plasmid (Takara, Tokyo, Japan) with a newly created *Mlu* I site at the multiple cloning site, yielding the plasmid pPrnd-EGFP. Next, two *Prnp* genomic DNAs, the 806-bp fragment from nt 18,861 to 19,667 encompassing a part of intron 2 and an entire 5′ UTR of exon 3 and the 1699-bp DNA from nt 20,442 to 22,140 consisting of an entire 3′ UTR and the downstream intervening sequence, were amplified by PCR. The former possessed the artificial *Spe* I and *Bam*H I enzyme sites at the 5′ and 3′ ends, respectively, and the latter contained the *Not* I and *Sal* I sites at the 5′ and 3′ ends, respectively. These fragments were ligated with the DsRed-coding *Bam*H I–*Not* I insert of pDsRed1-N1 (Clontech) in such a way that the insert was flanked by the two genomic fragments, and cloned into the *Spe* I and *Sal* I sites of pPrnd-EGFP, resulting in pPrPwild.

2.1.2. pPrP5′targeted

The 750-bp (from nt 18,661 to 19,411) fragment of *Prnp* intron 2, containing *Spe* I and *BamH* I sites at the 5′ and 3′ ends, respectively, was generated by PCR with a primer pair, and then placed for the corresponding fragment in pPrPwild, resulting in pPrP5′targeted.

2.1.3. pPrPint2(-3), pPrPint2(-26), pPrPint2(-50)

The *Prnp* intron 2 containing either 3-bp from nt 19,664 to 19,666, 26-bp from nt 19,641 to 19,666, or 50-bp from nt 19,617 to 19,666, together with the 5′ UTR of exon 3 and the

DsRed open reading frame (ORF), was amplified by PCR with a primer pair using pPrPwild as a template. *Bgl* II and *Not* I sites were introduced at the 5′ and 3′ ends of each fragment, respectively. These amplified fragments were placed for the corresponding fragment in pPrP5′targeted, respectively, yielding pPrPint2(-3), pPrPint2(-26) and pPrPint2(-50).

2.1.4. pPrP3′targeted and pPrPtargeted

A genomic fragment from nt 20,893 (corresponding to the *Eco*R I site in *Prnp* exon 3) to 22,140, encompassing a part of 3′ UTR and the downstream intervening sequence, was amplified by PCR using pPrPwild as a template with primers, each containing the *Not* I or *Sal* I recognition sequences. This amplified fragment was placed for the corresponding *Not* I–*Sal* I fragment in pPrPwild, producing a pPrP3′targeted plasmid. Moreover, pPrPtargeted was constructed by replacing this amplified fragment with the corresponding fragment in pPrP5′ targeted.

2.1.5. pPrPint2(-26)AG, pPrPint2(-26)Br, pPrPint2(-26)Br2×, pPrPint2(-26)AGBr2×

To construct these vectors, point mutations were introduced using a QuickChange Site-Directed Mutagenesis Kit (Stratagen, La Jolla, CA) using pPrPint2(-26) as a template. The mutations were verified by DNA sequencing.

2.2. Transfection and fluorescent microscopic analysis

Plasmids were transfected into mouse neuroblastoma N2a cells, which were maintained at 37 °C under 5% CO_2 in Dulbecco's Modified Eagle Medium (DMEM) supplemented with 10% fetal bovine serum. 2×10^5 cells were plated in one well of a 6-well plate and transfected by plasmids using Lipofectamin 2000 reagent (Invitrogen life technologies, Carlsbad, CA) the next day, as recommended by the manufacturer. Cells were inspected 48 h after transfection by fluorescence microscopy.

2.3. 3′ Rapid amplification of cDNA ends (RACE)

Total RNA was isolated from the cells 48 h after transfection using a Trizol reagent (Invitrogen life technologies). 1 μg of total RNA was subjected to first strand cDNA synthesis with Oligo dT-3 sites Adaptor Primer using the 3′-Full RACE Core Set (Takara) according to the manufacturer's recommendations. The synthesized cDNAs were subsequently amplified directly by PCR using the R-U5-3* primer, 5′-AGTGATTGACTACCC GTCAGCGGGGGTC-3′, and the 3 sites Adaptor Primer, 5′-CTGATCTAGAGGTACCGGATCC-3′.

2.4. DNA sequencing

DNA sequences were determined by the chain termination reaction method using Texas Red labeled specific primers (Amersham) and the ThermoSequenase premixed cycle sequencing kit (Amersham) according to the manufacturer's recommendations.

3. Results and discussion

3.1. Establishment of an in vitro transient transfection system to easily detect abnormal expression of PrPLP/Dpl by EGFP fluorescent protein

To establish an *in vitro* transient transfection system, in which the intergenic splicing-mediated abnormal expression of PrPLP/Dpl in ataxic lines of $Prnp^{0/0}$ mice can be mimicked in cultured cells, we first constructed two expression vectors, termed pPrPwild and pPrPtargeted. pPrPwild contained a part of *Prnp* genomic DNA including 816-bp of the 3′ part of intron 2, the entire exon 3, and the 3′ intervening sequence, followed by a *Prnd* genomic fragment comprising intron 1, exon 2, intron 2, exon 3 and the 3′ intervening sequence (Fig. 1B). In this vector, transcription is engineered to start from the upstream vector-derived exon under the control of the immediate early gene promoter of human cytomegalovirus (HCMV) and terminate at the end of *Prnp* exon 3 using its native poly(A) signal (Fig. 1B). We also replaced the *Prnp*- and *Prnd*-coding sequences with those of the fluorescent proteins, DsRed and EGFP, respectively (Fig. 1B), to easily detect expression of the *Prnp*- or the *Prnd*-coding exon under fluorescence microscopy. pPrPtargeted lacks the same *Prnp* region as in the ataxic lines of $Prnp^{0/0}$ mice, including 250-bp of intron 2, 10-bp of the 5′ UTR, the entire PrP ORF, and 450-bp of the 3′ UTR (Fig. 1A and B).

We then transfected these vectors into mouse N2a neuroblastoma cells and carried out a fluorescent microscopic examination 48 h after transfection. We also characterized the transcripts expressed from the vectors in these transfected cells by a 3′ RACE cloning technique and subsequent DNA sequencing. The pPrPwild-transfected cells produced DsRed fluorescence alone (Fig. 1C). No EGFP expression could be detected in these cells (Fig. 1C). 3′ RACE of the total RNA extracted from these transfected cells revealed several distinct bands, including one major and a few minor bands, on an agarose gel (Fig. 2A). We cloned the major band and determined its DNA sequence. The major transcript consisted of the vector-derived exon and *Prnp* exon 3 followed by a poly(A) tail (Fig. 2B), indicating that transcription was started from the vector-derived exon, terminating at the end of the *Prnp* exon 3, being subjected to splicing between these two exons. In contrast, pPrPtargeted produced only green EGFP but not DsRed fluorescence in the cells (Fig. 1C). 3′ RACE of these cells produced one major and a few minor bands on an agarose gel (Fig. 2A). DNA sequencing of the major band showed that it comprised the vector-derived exon and the downstream *Prnd* exons (Fig. 2B), indicating that the pre-mRNA started from the vector-derived exon was unsuccessfully terminated at the end of the *Prnp* terminal exon 3, elongated to the *Prnd* terminal exon 3, and subsequently underwent aberrant splicing between the vector-derived exon and the *Prnd* exons 2 and 3. This abnormal processing of the pre-mRNA expressed from pPrPtargeted in N2a cells is very similar to that for the targeted *Prnp* allele in the ataxic lines of $Prnp^{0/0}$ mice (Moore et al., 1999; Li et al., 2000a), whereas the processing for the pre-mRNA in the cells transfected

by pPrPwild is similar to that in wild-type mice. These results indicate that our newly established *in vitro* transient transfection system could reproduce the abnormal expression of PrPLP/Dpl in the ataxic lines of $Prnp^{0/0}$ mice in cultured cells by expression of EGFP fluorescent protein. Since pPrPtargeted lacks the *Prnp* sequences commonly targeted in the ataxic lines of $Prnp^{0/0}$ mice (Sakaguchi et al., 1995; Moore et al., 1999; Rossi et al., 2001), it is conceivable that the abnormal expression of PrPLP/Dpl in the ataxic lines of $Prnp^{0/0}$ mice is very likely due to deletion of a *cis*-element(s) present in the commonly targeted *Prnp* sequences.

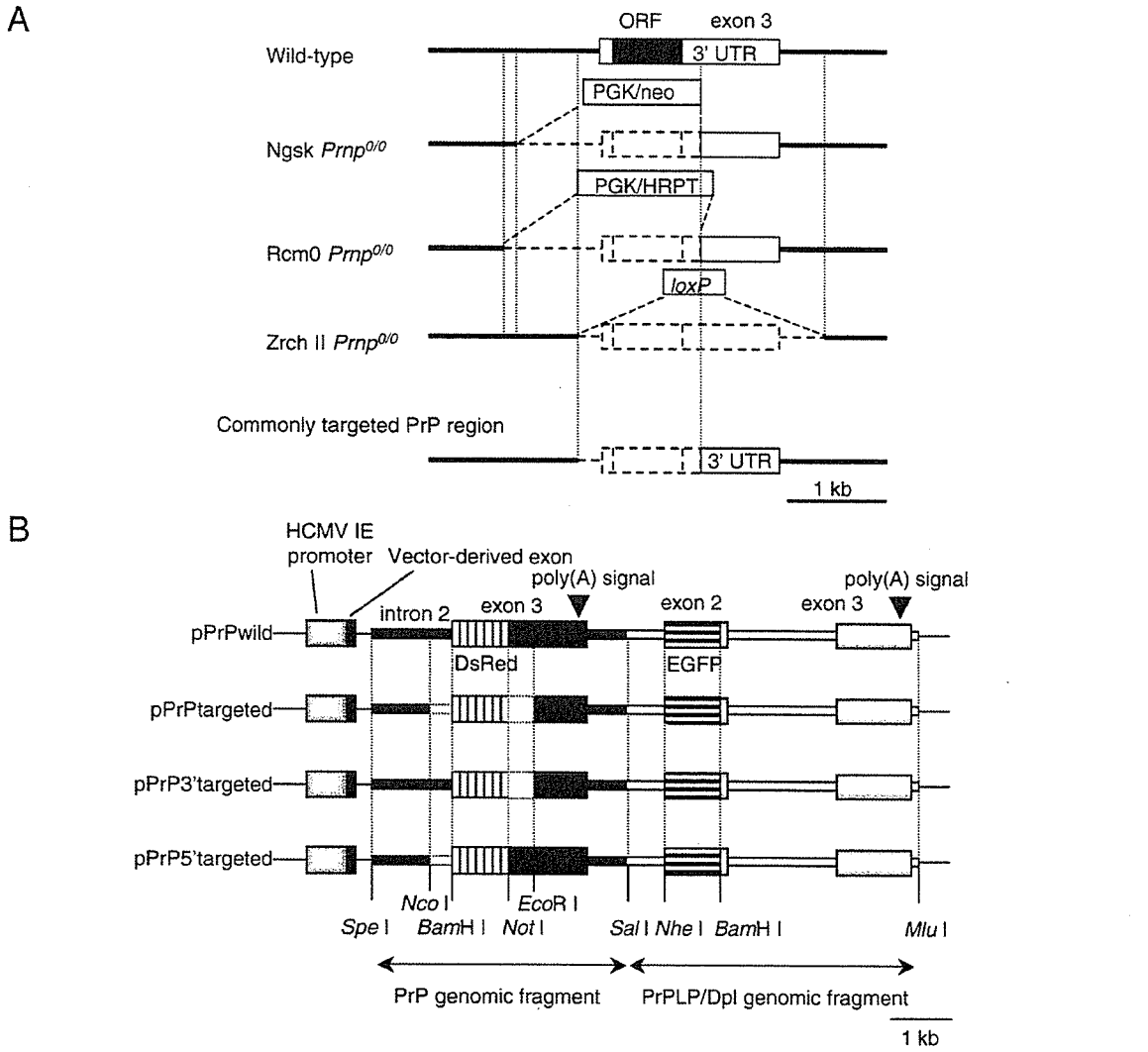

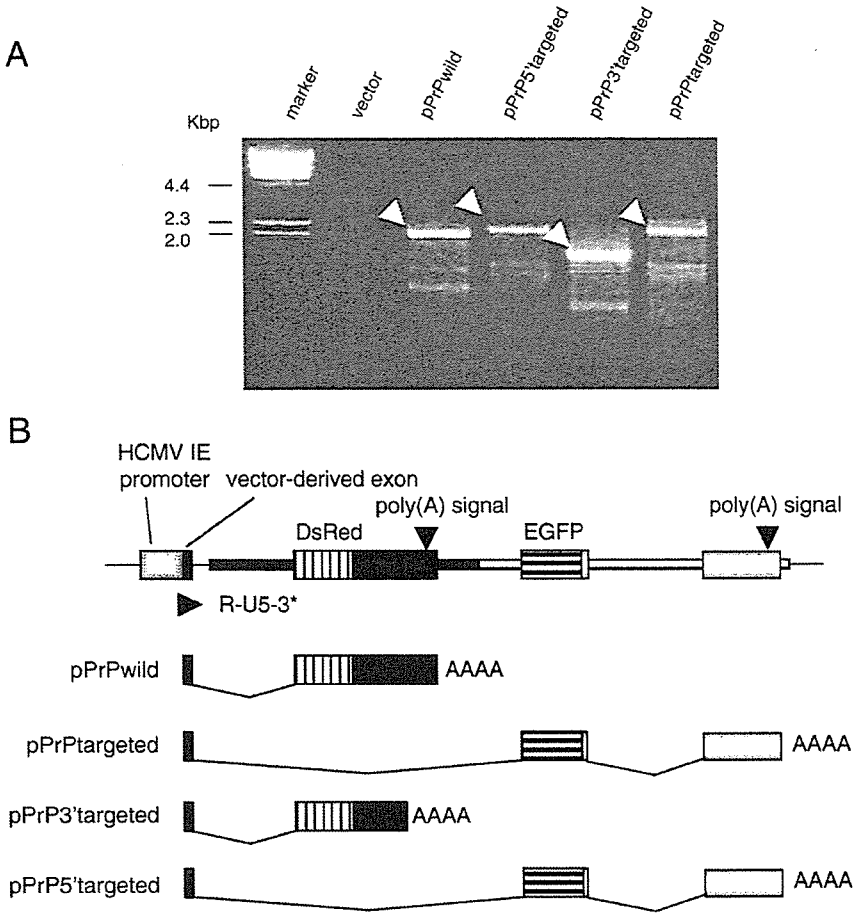

Fig. 2. (A) 3′ RACE of N2a cells 48 h after transient transfection of pPrPwild, pPrPtargeted, pPrP3′targeted, and pPrP5′targeted. Several distinct bands including one major band (indicated by arrow heads) are visible in each lane. (B) Schematic structures of the major transcripts expressed in the transfected N2a cells. These structures were determined on the basis of the DNA sequence of each major band. All poly(A) signals are native. AAAA indicates a poly(A) tail. R-U5-3* is a primer used for 3′ RACE.

3.2. Abnormal expression of PrPLP/Dpl assessed in the in vitro transient transfection system with vectors carrying various deletions in the upstream Prnp sequence

To employ our newly established *in vitro* system to investigate the genetic mechanism of the abnormal expression of PrPLP/Dpl in the ataxic lines of *Prnp*$^{0/0}$ mice, we constructed two other vectors, pPrP3′targeted and pPrP5′targeted. pPrP3′targeted lacks 450-bp of the *Prnp* 3′ UTR whereas pPrP5′targeted lacks 249-bp of intron 2 and 10-bp of the 5′ UTR (Fig. 1B). We transfected pPrP3′targeted and pPrP5′targeted into N2a cells. pPrP3′targeted expressed DsRed but not EGFP fluorescence in N2a cells 48 h after transfection (Fig. 1C). 3′ RACE and DNA sequencing showed that the major transcript expressed in these cells was composed of the vector-derived exon and the *Prnp* exon 3, similar to that in pPrPwild-transfected cells (Fig. 2A and B). This compositional similarity of the transcripts indicates that the pre-mRNAs expressed from pPrPwild and pPrP3′targeted are similarly processed in these transfected cells. Since pPrP3′targeted lacks the commonly targeted *Prnp* 3′ UTR, deletion of this part is unlikely to be involved in the

Fig. 1. (A) *Prnp* alleles in wild-type, Ngsk *Prnp*$^{0/0}$, Rcm0 *Prnp*$^{0/0}$, and Zrch II *Prnp*$^{0/0}$ mice. In Ngsk *Prnp*$^{0/0}$ mice, a 2.1-kb *Prnp* genomic DNA comprising 900-bp of intron 2, 10-bp of the 5′ UTR, an entire PrP ORF, and 450-bp of the 3′ UTR was replaced with a neomycin cassette (Sakaguchi et al., 1995). A similar part of *Prnp* was targeted in Rcm0 *Prnp*$^{0/0}$ mice (Moore et al., 1999). In Zrch II *Prnp*$^{0/0}$ mice, the *Prnp* genomic region consisting of 250-bp of intron 2, the entire exon 3, and 600-bp of the downstream intervening sequence was deleted (Rossi et al., 2001). Thus, 250-bp of intron 2 and a subsequent part of exon 3 including 10-bp of the 5′ UTR, the ORF, and 450-bp of the 3′ UTR are commonly targeted. (B) Schematic structures of the expression vectors, pPrPwild, pPrPtargeted, pPrP3′targeted, and pPrP5′targeted. pPrPwild was constructed by ligation of a PrP genomic fragment, including part of intron 2, exon 3, and the 3′ downstream sequence, and a PrPLP/Dpl genomic fragment including a part of intron 1, exon 2, intron 2, exon 3 and the 3′ downstream sequence in tandem under the control of the HCMV IE promoter. Each exon 3 contains a native poly(A) signal. The ORFs for PrP and PrPLP/Dpl are replaced with those for DsRed and EGFP, respectively. pPrPtargeted lacks the same part of *Prnp* as in the ataxic lines of *Prnp*$^{0/0}$ mice as indicated by the dotted square. pPrP3′targeted lacks 450-bp of the PrP 3′ UTR and pPrP5′targeted lacks 250-bp of intron 2 and 10-bp of the 5′ UTR. (C) Fluorescent microscopic photographs of mouse neuroblastoma N2a cells 48 h after transient transfection with pPrPwild, pPrPtargeted, pPrP3′targeted, and pPrP5′targeted.

abnormal regulation of *Prnd* in the ataxic lines of $Prnp^{0/0}$ mice. In contrast, pPrP5′targeted showed green EGFP fluorescence in the cells (Fig. 1B) and expressed the major transcript consisting of the vector-derived exon that was aberrantly spliced to the downstream *Prnd* exon 2 (Fig. 2A and B), similar to pPrPtargeted (Fig. 1B). These results indicate that our newly established *in vitro* transient transfection system is highly feasible to investigate the genetic mechanism of the abnormal expression of PrPLP/Dpl in the ataxic lines of $Prnp^{0/0}$ mice. pPrP5′targeted lacks 249-bp of intron 2 and 10-bp of the 5′ UTR. Thus, it is suggested that deletion of either 249-bp of intron 2 or 10-bp of the 5′ UTR or both in *Prnp* is responsible for the abnormal expression of downstream *Prnd* in the ataxic lines of $Prnp^{0/0}$ mice.

We further employed the *in vitro* system with several additional vectors, which were constructed by sequentially deleting 249-bp of intron 2 from the 5′ end. pPrPint2(-3) possesses only 3-bp of intron 2, including a splice acceptor of dinucleotides AG, and the subsequent 10-bp of the 5′ UTR (Fig. 3A). N2a cells transfected by this vector expressed EGFP, similar to those of pPrPtargeted and pPrP5′targeted (Fig. 3B), indicating that deletion of *Prnp* intron 2 is responsible for the abnormal expression of *Prnd*-coding exon in the transfected cells. In contrast, pPrPint2(-26) and pPrPint2(-50), containing 3′ 26- and 50-bp of intron 2, respectively, together with 10-bp of the 5′ UTR, exhibited DsRed signals in the cells (Fig. 3A and B). These results indicate that the unsuccessful cleavage/polyadenylation-mediated abnormal expression of *Prnd*-coding exon in the transfected cells is attributable to deletion of at least the 3′ 26-bp of *Prnp* intron 2. It is also suggested that lack of the same sequence in *Prnp* is responsible for the abnormal expression of PrPLP/Dpl in the ataxic lines of $Prnp^{0/0}$ mice.

3.3. The in vitro transient transfection system visualizes the functional disconnection of the pre-mRNA machineries underlying the abnormal expression of PrPLP/Dpl

Within the 26-bp intronic sequence, various elements important for pre-mRNA splicing, including a splice branch point, a polypyrimidine tract, and a splice acceptor are present. To investigate whether disruption of these elements could be involved in the impairment of pre-mRNA cleavage/polyadenylation at the end of *Prnp* leading to EGFP expression, we introduced various point mutations into the splice acceptor and/or the branch point in pPrPint2(-26). pPrPint2(-26)AG, carrying a G to T mutation in both the authentic splice acceptor AG and the adjacent downstream cryptic AG in the 5′ UTR, showed expression of EGFP in the cells (Fig. 4A and B). pPrPint2(-26)AGBr2× including mutations in all of these branch points and splice acceptors similarly expressed EGFP in the cells (Fig. 4A and B). These results clearly indicate that disruption of the splice acceptor in *Prnp* intron 2 caused expression of the downstream EGFP-coding exon. In contrast, pPrPint2(-26)Br carries an A to T mutation at the authentic branch point and expressed DsRed in the transfected N2a cells (Fig. 4A and B). Similar DsRed expression was observed in the cells transfected by pPrPint2(-26)Br2×, which contained an additional A to G mutation at the 2-bp downstream cryptic branch point (Fig. 4A and B). Therefore,

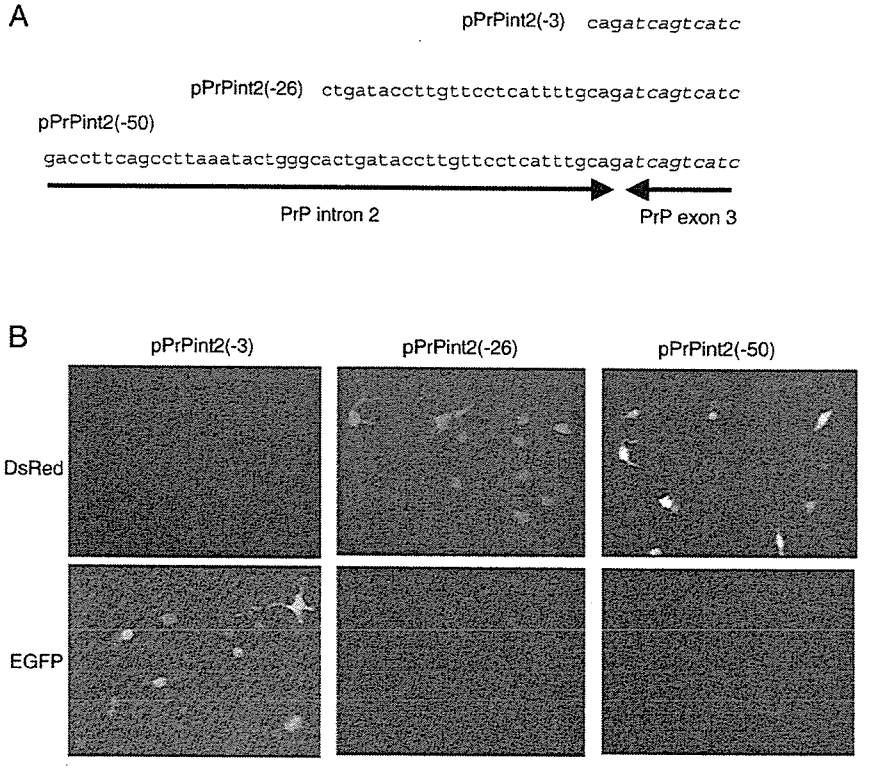

Fig. 3. (A) Nucleotide sequences of PrP intron 2 and exon 3 in pPrPint2(-3), pPrPint2(-26), and pPrPint2(-50). Italic letters are nucleotides in exon 3. (B) Fluorescent microscopic photographs of N2a cells 48 h after transient transfection with pPrPint2(-3), pPrPint2(-26), and pPrPint2(-50).

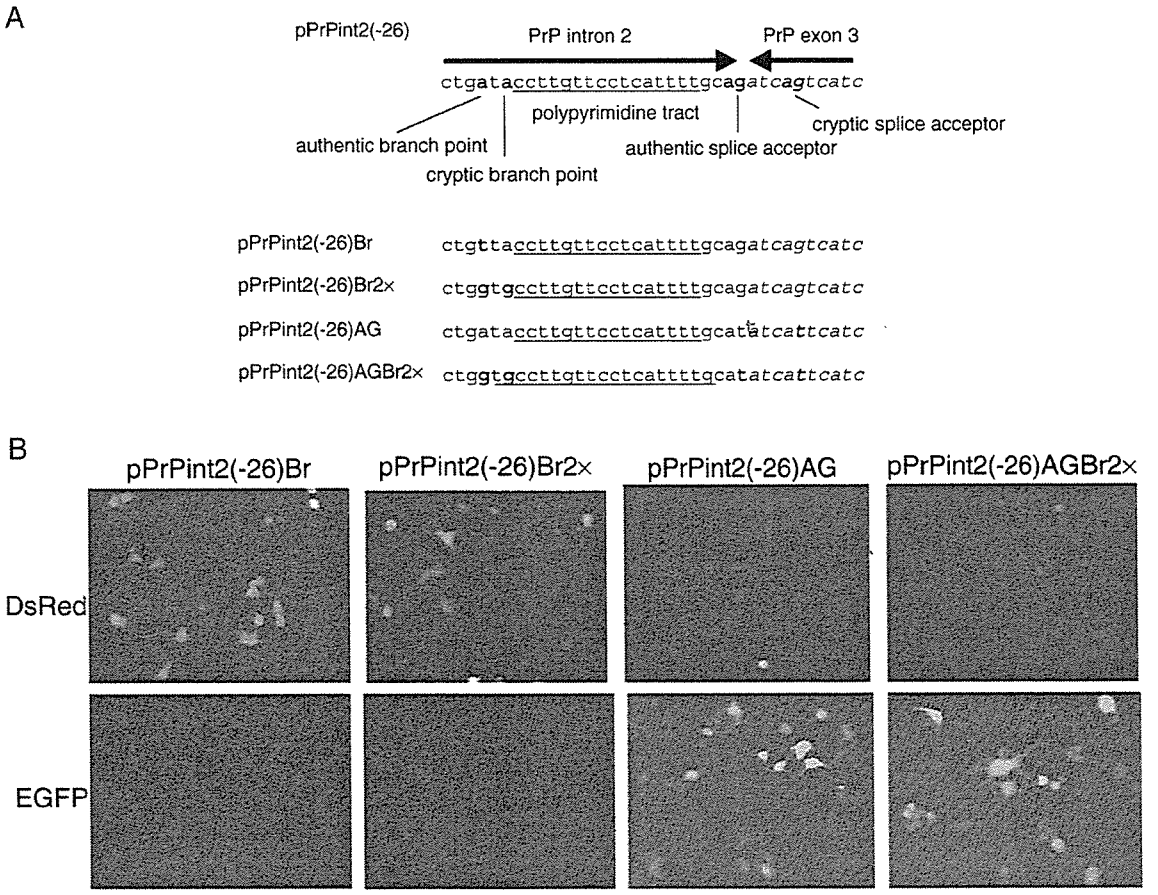

Fig. 4. (A) Point mutations introduced in the splice elements of pPrPint2(-26)Br, pPrPint2(-26)Br2×, pPrPint2(-26)AG, and pPrPint2(-26)AGBr2×. Nucleotide sequences in PrP intron 2 and exon 3 of pPrPint2(-26) are shown, including authentic and cryptic branch points, splice acceptors and a polypyrimidine tract. Mutated nucleotides are shown in bold letters. (B) Fluorescent microscopic photographs of N2a cells 48 h after transient transfection with pPrPint2(-26)Br, pPrPint2(-26)Br2×, pPrPint2(-26)AG, and pPrPint2(-26)AGBr2×.

it appears that lack of the functional branch point is unlikely to be involved in the abnormal expression of *Prnd*. However, pPrPint2(-3), which possesses the splice acceptor but lacks the branch point and polypyrimidine tract, expressed EGFP in N2a cells (Fig. 3B), indicating that deletion of the branch point or polypyrimidine tract might also be responsible for the expression of EGFP. It is thus possible that the expression of DsRed in the cells transfected by pPrPint2(-26)Br or pPrPint2(-26)Br2× is due to the presence of other functional cryptic branch points. Taken together, these results indicate that collapse in the integrity of splicing machineries could be responsible for the expression of EGFP in the cells by causing the impaired cleavage/polyadenylation of pre-mRNA. It is recently believed that splicing of the terminal intron is functionally linked to the cleavage/polyadenylation of pre-mRNA during transcription (Steinmetz, 1997; Proudfoot et al., 2002; Kornblihtt et al., 2004). It is therefore very likely that the functional disconnection of pre-mRNA machineries, in particular those of splicing and cleavage/polyadenylation, underlies the abnormal expression of PrPLP/Dpl in the ataxic lines of $Prnp^{0/0}$ mice. More importantly, these results indicate that our established *in vitro* transient transfection system is very useful to easily detect the functional disconnection of the pre-mRNA machineries from the expression of the EGFP fluorescent protein under fluorescence microscopy.

Splicing is mediated by a large molecular complex, splicesome, consisting of small nuclear ribonucleoproteins (snRNPs) and non-RNP splicing factors of a SR protein family (Proudfoot et al., 2002). The cleavage/polyadenylation of pre-mRNA is also regulated by various factors, including poly(A) polymerase (PAP), cleavage/polyadenylation specificity factor (CPSF), and cleavage stimulatory factor (Wahle and Ruegsegger, 1999; Proudfoot et al., 2002). U2AF is a dimeric splicing factor, interacting with the splice acceptor and polypyrimidine tract and helping recruit the U2 snRNP to the branch point together with a branch point binding protein (Vagner et al., 2000). It has been shown that PAP can interact with the large subunit of U2AF, U2AF65, and stimulate pre-mRNA splicing *in vivo* (Vagner et al., 2000). It was also reported that U2AF65 increased 3′-end cleavage efficiency (Millevoi et al., 2002). It is therefore conceivable that U2AF is a key molecule functionally connecting splicing and cleavage/polyadenylation. However, the molecular mechanism of how the pre-mRNA machineries are functionally connected to each other remains to be investigated.

Thus, our newly established *in vitro* transient transfection system might be employed to investigate the mechanism of the functional connection between the pre-mRNA machineries.

Recently, it has been shown that some viral proteins can disturb the function of pre-mRNA machineries by interacting with their components. Influenza virus NS1 protein was shown to inhibit cleavage/polyadenylation processes of cellular pre-mRNA by interacting with the 30 kDa subunit of CPSF (Nemeroff et al., 1998). Shimizu et al. subsequently reported that transcripts for the major heat shock protein HSP70, and β-actin were elongated due to the insufficient cleavage of these corresponding pre-mRNAs in influenza virus-infected cells (Shimizu et al., 1999). It was also shown that Epstein–Barr virus protein nuclear antigen 5 could inhibit cleavage/polyadenylation of cellular pre-mRNA (Dufva et al., 2002), and that human cytomegalovirus infection altered splicing and polyadenylation of cellular pre-mRNA (Adair et al., 2004). Interestingly, it was shown that Tgat, an oncogenic protein, was newly generated probably due to the impaired pre-mRNA processing in adult T-cell leukemia, the disease caused by human T-cell leukemia virus (Yoshizuka et al., 2004). Therefore, our newly established system may also be applied to elucidation of the molecular pathogenesis of pathological conditions.

3.4. Conclusions

In this study, we newly established an *in vitro* transient transfection system in which the functional disconnection of the pre-mRNA machineries could easily be detected by the expression of EGFP fluorescent protein under fluorescence microscopy. Employing this system, we showed that the abnormal expression of PrPLP/Dpl in ataxic lines of *Prnp*$^{0/0}$ mice can be visualized by expression of the green fluorescence protein EGFP in cultured cells, and identified that the abnormal expression of PrPLP/Dpl is probably due to functional disconnection between the pre-mRNA machineries, in particular those of splicing and cleavage/polyadenylation. Therefore, our newly established *in vitro* system might be useful to investigate the molecular mechanisms of the functional connection between the pre-mRNA machineries in normal and pathological conditions.

Acknowledgement

This study was supported in part by a Research on Specific Diseases grant from the Ministry of Health, Labour and Welfare, Japan.

References

Adair, R., Liebisch, G.W., Su, Y., Colberg-Poley, A.M., 2004. Alteration of cellular RNA splicing and polyadenylation machineries during productive human cytomegalovirus infection. J. Gen. Virol. 85, 3541–3553.

Anderson, L., Rossi, D., Linehan, J., Brandner, S., Weissmann, C., 2004. Transgene-driven expression of the Doppel protein in Purkinje cells causes Purkinje cell degeneration and motor impairment. Proc. Natl. Acad. Sci. U. S. A. 101, 3644–3649.

Behrens, A., et al., 2002. Absence of the prion protein homologue Doppel causes male sterility. EMBO J. 21, 3652–3658.

Bueler, H., et al., 1992. Normal development and behaviour of mice lacking the neuronal cell-surface PrP protein. Nature 356, 577–582.

Dufva, M., Flodin, J., Nerstedt, A., Ruetschi, U., Rymo, L., 2002. Epstein–Barr virus nuclear antigen 5 inhibits pre-mRNA cleavage and polyadenylation. Nucleic Acids Res. 30, 2131–2143.

Kornblihtt, A.R., de la Mata, M., Fededa, J.P., Munoz, M.J., Nogues, G., 2004. Multiple links between transcription and splicing. RNA 10, 1489–1498.

Li, A., et al.,.2000a. Identification of a novel gene encoding a PrP-like protein expressed as chimeric transcripts fused to PrP exon 1/2 in ataxic mouse line with a disrupted PrP gene. Cell. Mol. Neurobiol. 20, 553–567.

Li, A., et al., 2000b. Physiological expression of the gene for PrP-like protein, PrPLP/Dpl, by brain endothelial cells and its ectopic expression in neurons of PrP-deficient mice ataxic due to Purkinje cell degeneration. Am. J. Pathol. 157, 1447–1452.

Manson, J.C., Clarke, A.R., Hooper, M.L., Aitchison, L., McConnell, I., Hope, J., 1994. 129/Ola mice carrying a null mutation in PrP that abolishes mRNA production are developmentally normal. Mol. Neurobiol. 8, 121–127.

Millevoi, S., Geraghty, F., Idowu, B., Tam, J.L., Antoniou, M., Vagner, S., 2002. A novel function for the U2AF 65 splicing factor in promoting pre-mRNA 3′-end processing. EMBO Rep. 3, 869–874.

Moore, R.C., et al., 1999. Ataxia in prion protein (PrP)-deficient mice is associated with upregulation of the novel PrP-like protein Doppel. J. Mol. Biol. 292, 797–817.

Moore, R.C., et al., 2001. Doppel-induced cerebellar degeneration in transgenic mice. Proc. Natl. Acad. Sci. U. S. A. 98, 15288–15293.

Nemeroff, M.E., Barabino, S.M., Li, Y., Keller, W., Krug, R.M., 1998. Influenza virus NS1 protein interacts with the cellular 30 kDa subunit of CPSF and inhibits 3′end formation of cellular pre-mRNAs. Mol. Cell 1, 991–1000.

Proudfoot, N.J., Furger, A., Dye, M.J., 2002. Integrating mRNA processing with transcription. Cell 108, 501–512.

Rossi, D., et al., 2001. Onset of ataxia and Purkinje cell loss in PrP null mice inversely correlated with Dpl level in brain. EMBO J. 20, 694–702.

Sakaguchi, S., et al., 1995. Accumulation of proteinase K-resistant prion protein (PrP) is restricted by the expression level of normal PrP in mice inoculated with a mouse-adapted strain of the Creutzfeldt–Jakob disease agent. J. Virol. 69, 7586–7592.

Sakaguchi, S., et al., 1996. Loss of cerebellar Purkinje cells in aged mice homozygous for a disrupted PrP gene. Nature 380, 528–531.

Shimizu, K., Iguchi, A., Gomyou, R., Ono, Y., 1999. Influenza virus inhibits cleavage of the HSP70 pre-mRNAs at the polyadenylation site. Virology 254, 213–219.

Steinmetz, E.J., 1997. Pre-mRNA processing and the CTD of RNA polymerase II: the tail that wags the dog? Cell 89, 491–494.

Vagner, S., Vagner, C., Mattaj, I.W., 2000. The carboxyl terminus of vertebrate poly(A) polymerase interacts with U2AF 65 to couple 3′-end processing and splicing. Genes Dev. 14, 403–413.

Wahle, E., Ruegsegger, U., 1999. 3′-End processing of pre-mRNA in eukaryotes. FEMS Microbiol. Rev. 23, 277–295.

Yamaguchi, N., Sakaguchi, S., Shigematsu, K., Okimura, N., Katamine, S., 2004. Doppel-induced Purkinje cell death is stoichiometrically abrogated by prion protein. Biochem. Biophys. Res. Commun. 319, 1247–1252.

Yoshizuka, N., et al., 2004. An alternative transcript derived from the trio locus encodes a guanosine nucleotide exchange factor with mouse cell-transforming potential. J. Biol. Chem. 279, 43998–44004.

Surface Plasmon Resonance Analysis for the Screening of Anti-prion Compounds

Satoshi KAWATAKE,[a] Yuki NISHIMURA,[a] Suehiro SAKAGUCHI,[b] Toru IWAKI,[c] and Katsumi DOH-URA*,[a]

[a] *Department of Prion Research, Tohoku University; Sendai 980–8575, Japan:* [b] *Department of Molecular Microbiology and Immunology, Nagasaki University; Nagasaki 852–8523, Japan: and* [c] *Department of Neuropathology, Neurological Institute, Kyushu University; Fukuoka 812–8582, Japan.*

Received November 2, 2005; accepted January 24, 2006; published online January 27, 2006

The interaction of anti-prion compounds and amyloid binding dyes with a carboxy-terminal domain of prion protein (PrP121—231) was examined using surface plasmon resonance (SPR) and compared with inhibition activities of abnormal PrP formation in scrapie-infected cells. Most examined compounds had affinities for PrP121—231: antimalarials had low affinities, whereas Congo red, phthalocyanine and thioflavin S had high affinities. The SPR binding response correlated with the inhibition activity of abnormal PrP formation. Several drugs were screened using SPR to verify the findings: propranolol was identified as a new anti-prion compound. This fact indicates that drug screenings by this assay are useful.

Key words anti-prion compound; surface plasmon resonance; scrapie-infected cell; screening; recombinant prion protein

Transmissible spongiform encephalopathies or prion diseases are fatal neurodegenerative disorders that include Creutzfeldt–Jakob disease and Gerstmann–Sträussler–Scheincker syndrome in humans, and scrapie, bovine spongiform encephalopathy and chronic wasting disease in animals. These disorders are characterized by accumulation in the brain of an abnormal isoform of prion protein (PrP), which includes a high beta-sheet content and is resistant to digestion with proteinase K.[1] Recent outbreaks of variant Creutzfeldt–Jakob disease[2] and iatrogenic Creutzfeldt–Jakob disease through use of cadaveric growth hormone or dura grafts[3] in younger people have necessitated the development of suitable therapies. Compounds such as antimalarials and amyloid binding dyes are known to possess anti-prion activity *in vitro* or *in vivo*.[4—14] Among them, Congo red and quinacrine are known to bind directly to PrP and thereby strongly inhibit proteinase K-resistant PrP (PrPres) formation.[15,16] However, it remains unclear whether or not other anti-prion compounds and amyloid binding dyes interact directly with PrP. This study analyzed interactions of some previously reported anti-prion compounds[4,7,11,17,18] and popularly used amyloid binding dyes with recombinant PrP using surface plasmon resonance (SPR). In addition, we evaluated whether SPR assay is useful as a screening tool for anti-prion compounds.

MATERIALS AND METHODS

Compounds Compounds used in the study (Fig. 1) were obtained from Sigma Aldrich Corp. (quinacrine dihydrochloride (QC, MW: 400.0), quinine hydrochloride (QN, MW: 324.4), thioflavin T (ThT, MW: 283.4, dye content 65%), thioflavin S (ThS, MW: undetermined), propranolol (MW: 295.8), promethazine hydrochloride (MW: 284.4), carbamazepine (MW: 236.3) and theophylline (MW: 180.2)), Aldrich (chloroquine diphosphate (CQ, MW: 319.9), and Congo red (CR, MW: 696.7, dye content 97%)), ICN (phthalocyanine tetrasulfonate (PcTS, MW: 922.7)), Wako Pure Chemical Industries Ltd. (Tokyo, Japan) (tetracycline hydrochloride (TC, MW: 444.4), diazepam (MW: 284.7), folic acid (MW: 441.4) and phenytoin (MW: 252.3)) or Nacalai Tesque (Tokyo, Japan) (testosterone (MW: 288.4)). All compounds were prepared as 20 mM stock solutions in water or dimethyl sulfoxide.

SPR Analysis The SPR analysis was performed using an

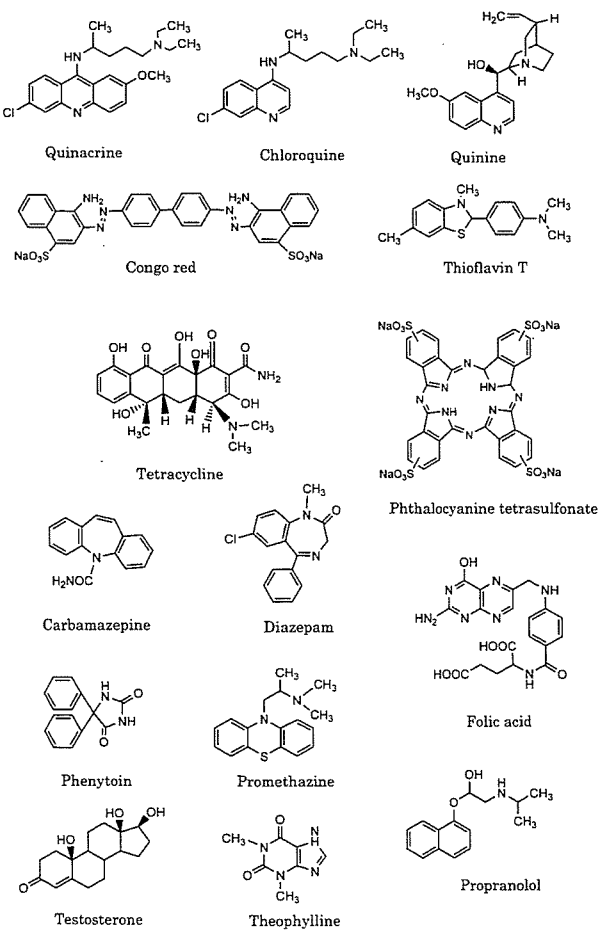

Fig. 1. Structures of Compounds or Drugs Used in the Study

* To whom correspondence should be addressed. e-mail: doh-ura@mail.tains.tohoku.ac.jp

optical biosensor (Biacore AB, Uppsala, Sweden) equipped with a CM5 sensor chip. Recombinant mouse PrP was prepared as described previously[19,20] and immobilized on a biosensor chip at a density of *ca.* 3000 resonance units (RU) using amine coupling.[21] Test compounds were diluted to 100 μM with running buffer (70 mM NaCl, 53 mM Na_2HPO_4, 12.5 mM KH_2PO_4, pH 7.4) and contained 0.5% DMSO. After they were confirmed to be in solution without precipitation or aggregation, they were injected over the PrP flow cell and the reference for either 60 s at a flow rate of 20 μl/min (low-affinity compounds) or 90 s at a flow rate of 30 μl/min (high-affinity compounds). The dissociation phase was monitored for 60 s (low-affinity compounds) or 270 s (high-affinity compounds). The flow cell was washed with 10 mM NaOH or 0.01% Triton X-100 for 30 s between each sample injection. Buffer blanks for double referencing were injected before sample analyses.[22]

The full-length recombinant of mouse PrP (residues 23—231) was used initially in the experiment, but it was easily degraded during SPR analysis in the amino-terminal portions attributable to an unidentified mechanism. For that reason, the carboxy-terminal polypeptide (residues 121—231; PrP121—231), which represents the only autonomous folding unit of PrP with a defined three-dimensional structure,[19,23,24] was used in this study.

Every PrP-immobilized biosensor chip used in the study was confirmed to respond almost the same and was standardized by the measurement of QC before its use for sample analyses.

Data Analysis The binding response, which is an index for estimating the interaction of a compound with molecules sited on a biosensor chip, is obtained from the equilibrium response (R_{eq}) value or the maximum response value in the sensorgram divided by the molecular weight.[25] In this study, the binding response of a compound was standardized by calibrating with QC, whose binding response was designated as 100 RU/Da. For low-affinity compounds, the dissociation constant (K_D) based on the R_{eq} state was calculated from data at doses ranging from 10 μM to 1 mM by either steady-state analysis using BIAevaluation software (ver. 3.0; Biacore AB) or Scatchard plot analysis. On the other hand, the K_D for high-affinity compound CR or PcTS was deduced after the data were fit to a binding model assuming a bivalent analyte in BIAevaluation software. The fitting was performed in such a way that the χ^2 value representing the statistical closeness of curve-fitting became the lowest. It was recommended ideally to be below 10.

Statistical linear correlation was evaluated using Pearson's correlation coefficient; Fisher's r to z method was used to calculate the p values. Simple linear regression analysis was also performed.

Anti-prion Activity Assay Anti-prion activity of a compound was assayed by measuring its 50% inhibition doses (IC_{50}) for PrPres formation in scrapie-infected neuroblastoma (ScNB) cells as described in previous reports.[7,11,12] Briefly, compounds were added at designated concentrations to the medium when cells were passed at 10% confluency. Cells were allowed to grow to confluence and lysed with lysis buffer (0.5% sodium deoxycholate, 0.5% Nonidet P-40, PBS). Lysates were digested with 10 μg/ml proteinase K for 30 min and centrifuged at 100000×g for 30 min at 4 °C. The pellets were resuspended in sample loading buffer and boiled. Samples were separated using electrophoresis on a 15% Tris-glycine-SDS-polyacrylamide gel and electroblotted. PrPres was detected using an antibody SAF83 (1 : 5000; SPI-Bio, France), followed by an alkaline phosphatase-conjugated secondary antibody. Immunoreactive signals were visualized using CDP-Star detection reagent (Amersham Biosciences Corp., U.S.A.) and were analyzed densitometrically. Three independent assays were performed in each experiment.

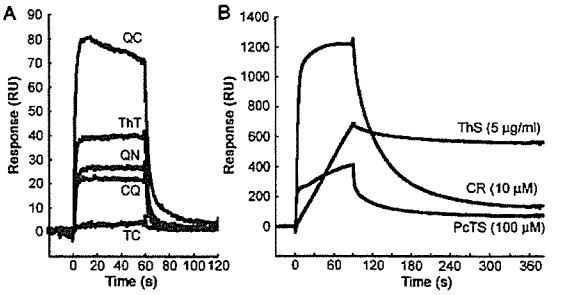

Fig. 2. Interactions of Anti-prion Compounds with PrP121—231

(A) Sensorgrams of the low-affinity compounds quinacrine (QC), chloroquine (CQ), quinine (QN), thioflavin T (ThT) and tetracycline (TC), all at 100 μM. (B) Sensorgrams of the high-affinity compounds Congo red (CR, 10 μM), phthalocyanine tetrasulfonate (PcTS, 100 μM) and thioflavin S (ThS, 5 μg/ml).

RESULTS

Interaction of Anti-prion Compounds with PrP The SPR sensorgrams of ThT and antimalarials such as QC, QN and CQ (each at 100 μM) demonstrated weak signal responses of less than 100 RU (Fig. 2A). The responses of these compounds reached equilibrium (R_{eq}) within a few seconds and returned to the baseline very rapidly after dissociation. These sensorgrams were typical for low-affinity interactions: TC showed almost no response. On the other hand, all sensorgrams of high-affinity compounds, such as CR, PcTS and ThS, showed much stronger responses and individual characteristic curves that differed from those of the low-affinity compounds (Fig. 2B). The CR (10 μM) showed the strongest signal, which was greater than 1200 RU: this decreased very slowly in the dissociation phase. The signal responses for PcTS (100 μM) and ThS (5 μg/ml) showed that neither reached the R_{eq} state within the association phase or returned to the baseline within the dissociation phase. In particular, ThS was only slightly dissociated and remained bound. This sensorgram resembled the sensorgram of biquinoline, an effective inhibitor of PrPres formation in ScNB cells (IC_{50}=3 nM).[11]

K_D Determination The dose response curve for QC appeared to be monophasic and to reach a saturation level at higher concentrations; its dissociation constant (K_D) value was calculated as 1.1 mM or 0.9 mM using steady-state analysis or Scatchard plot analysis, respectively (Figs. 3A—C). Vogtherr *et al.*[16] reported the dissociation constant (K_D= 4.6 mM) of the complex of QC and human PrP 121—230 analyzed by nuclear magnetic resonance (NMR) spectroscopy. This value was almost comparable to the K_D value obtained in this study, indicating that the method used in this study was relevant. The other two low-affinity compounds, QN and

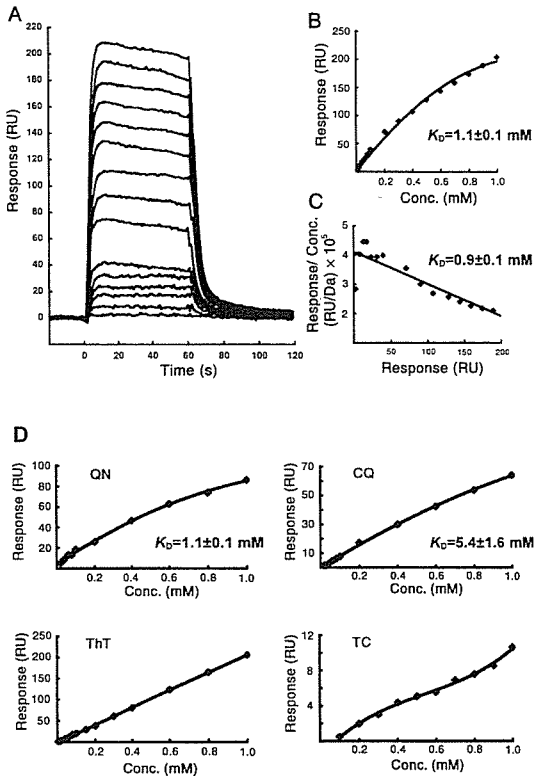

Fig. 3. Kinetic Analyses of Low Affinity Compounds

(A) Sensorgrams, (B) dose response curve and (C) scatchard plot of QC. (D) Dose response curves of QN, CQ, ThT, and TC.

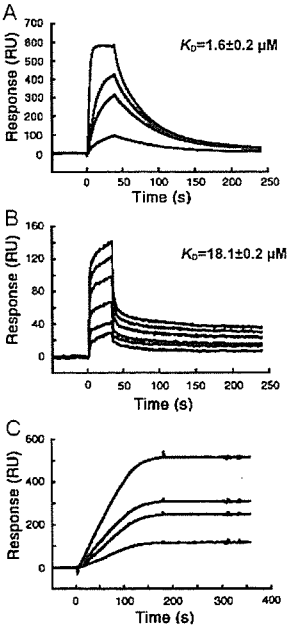

Fig. 4. Kinetic Analyses of High Affinity Compounds

(A) Sensorgrams of CR at concentrations of 1, 2, 3.3 and 5 μM, and its K_D value. (B) Sensorgrams of PcTS at concentrations of 1, 5, 10, 50, 75 and 100 μM, and its K_D value. (C) Sensorgrams of ThS at concentrations of 1, 2, 3 and 5 μg/ml, and its K_D value could not be calculated because of its undetermined structure and molecular weight.

CQ, respectively showed a similar monophasic pattern in dose response curves, yielding K_D of 1.1 mM and 5.4 mM (Fig. 3D). These K_D values, however, were of rough estimation and might be a little underscored due to lack of the data at concentrations of more than 1 mM. Unstable solubility of the compounds at such high concentrations hindered further analyses.

On the other hand, ThT gave a linear dose–response curve within a concentration of up to 1 mM and TC showed a biphasic pattern (Fig. 3D). Therefore, the saturation levels and K_D values of these compounds could not be determined, indicating that these compounds have a very low or no affinity with PrP121—231. Of them, TC is known to revert abnormal physicochemical properties of PrPres *in vitro*,[18] and interaction between TC and human PrP 106—126 peptides is revealed by NMR analysis.[26] Their data appear to be inconsistent with the data in this study. However, this discrepancy might be attributable to the lack of a TC binding site in the PrP121—231 used in our study.

Each sensorgram of high affinity compounds showed a very slow dissociation phase and was individually characteristic (Fig. 4). The structural and stoichiometric binding details of the compounds with PrP121—231 have not yet been established, but CR or PcTS is a symmetrical molecule and either half of the molecule has anti-prion activity (Doh-ura K, unpublished data). Consequently, the K_D value for the compound was deduced after the data were fit to a binding model assuming a bivalent analyte. The K_D of CR was calculated to be 1.6 μM from the sensorgrams of 1, 2, 3.3 and 5 μM (χ^2=20.9±2.1) (Fig. 4A). The K_D of PcTS was calculated as 18.1 μM from the sensorgrams of 1, 5, 10, 50, 75 and 100 μM (χ^2=28.1±2.9) (Fig. 4B). The K_D of ThS was incalculable to an exact degree because it is presumed to be a mixture of compounds formed by methylation and sulfonation of primulin; their structures and molecular weights have not been determined.

Comparison between PrP Affinity and Anti-prion Activity The IC_{50} value for the inhibition of PrPres formation in ScNB cells, either previously reported or examined in this study, was used as an anti-prion activity in this study. It was compared with the K_D or with the binding response. The latter, an index for estimating the interaction, was obtained from the R_{eq} value or the maximum response value at a concentration of 1 mM divided by the molecular weight (Table 1).

From data of all compounds except ThT, TC and ThS, statistical analyses demonstrated a significant linear correlation between the reciprocal of binding response and the IC_{50} (r=0.985, p=0.0005) (Fig. 5). This relation appeared to be also observed in TC, but not in ThT showing the next highest binding response to QC but no inhibition of PrPres formation within a non-toxic dose range. However, ThT demonstrated cell-toxicity at such a low dose as 0.05 μM.

For ThS, assuming that its minimum molecular weight deduced from presumable structures was 520 Da, its binding response was estimated to be 5.03 RU/Da; the IC_{50} was estimated to be about 2 μM, corresponding to about 1 μg/ml. However, these values seem to be underestimates because some constituents of ThS might interact with PrP121—231 or have inhibitory activity for PrPres formation. Therefore, active constituents of ThS might be expected to inhibit PrPres formation in ScNB cells at a submicromolar dose, similar to the other high-affinity compounds.

Screening by SPR Findings suggested that a compound

Table 1. Binding Response, Dissociation Constant (K_D) and 50% PrPres Inhibition Dose in ScNB Cells (IC_{50})

Compound	Binding response[a] (RU/Da)	K_D[b] (mM)	IC_{50}[c] (μM)
Low-affinity			
Quinacrine (QC)	0.25±0.00	1.1±0.1 (0.9±0.1)	0.3 (7)
Quinine (QN)	0.05±0.00	1.1±0.1 (1.4±0.1)	6.0 (11)
Chloroquine (CQ)	0.07±0.01	5.4±1.6 (3.5±0.8)	4.0 (7)
Thioflavin T (ThT)	0.16±0.01	n.d.[d] (n.d.[d])	No effect[f]
Tetracycline (TC)	0.01±0.00	n.d.[d] (n.d.[d])	No effect[g]
High-affinity			
Congo red (CR)	8.74±0.64	$1.6\pm0.2\times10^{-3}$	1.5×10^{-2} (4)
Phthalocyanine tetrasulfonate (PcTS)	1.82±0.06	$18.1\pm0.2\times10^{-3}$	0.5 (17)
Thioflavin S (ThS)	n.d.[e]	n.d.[e]	*ca.* 1 μg/ml

a) Binding response value was calculated from the R_{eq} value divided by the molecular weight for QC, QN, CQ and CR, or from the response value at a concentration of 1 mM divided by the molecular weight for ThT, TC and PcTS. *b*) K_D values were determined by steady state analysis for the low-affinity compounds or by bivalent analyte model analysis for CR and PcTS. K_D values from Scatchard plot analyses are shown in parentheses. *c*) IC_{50} values reported in the literature (reference shown in parentheses) or examined in this study. *d*) n.d.: not determined because a saturation level could not be estimated. *e*) n.d.: not determined because its structure and molecular weight were undetermined. *f*) Inhibition of PrPres formation was not observed up to a minimal toxic dose of 0.05 μM. *g*) Inhibition of PrPres formation was not observed up to a minimal toxic dose of 5.0 μM.

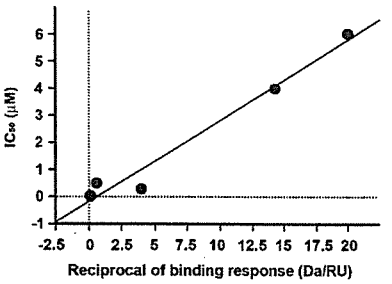

Fig. 5. Correlation between the Reciprocal of Binding Response and the IC_{50}

The data were from five compounds in which both binding response and IC_{50} were determined. Correlation showed a slope of 0.298, an intercept of −0.156 and a correlation coefficient of 0.971 (p=0.002) by simple linear regression analysis.

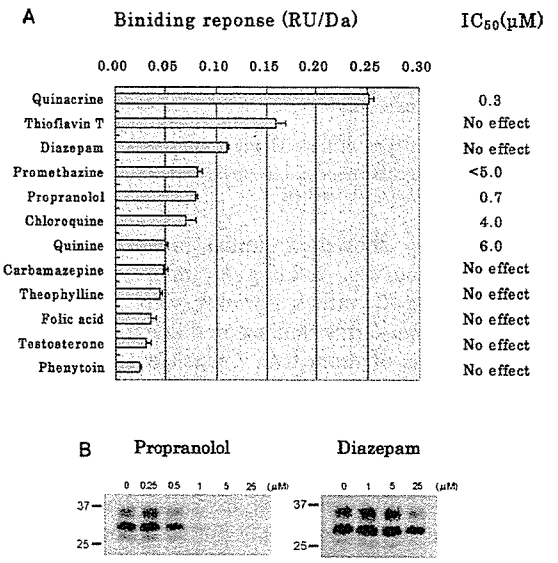

Fig. 6. Screening of Anti-prion Candidates Using the SPR Assay

(A) Binding response of each sample at 100 μM, and its IC_{50} of PrPres formation inhibition in ScNB cells within a non-toxic dose range. (B) Inhibition analyses of PrPres formation in ScNB cells grown in the presence with propranolol or diazepam. Molecular sizes in kDa are shown at the left of each panel.

capable of interacting with PrP121—231 might have a potency of inhibiting PrPres formation in ScNB cells. To verify this inference, several drugs were examined for either their binding response using the SPR method or their IC_{50} in ScNB cells. Eight clinically utilized drugs—carbamazepine, diazepam, folic acid, phenytoin, promethazine, propranolol, testosterone, and theophylline—all of which are low molecular weight compounds capable of crossing the blood brain barrier and share a partial structure similarity with the anti-prion compounds already reported, were examined and compared with the four anti-prion compounds (QC, QN, CQ, and ThT) (Fig. 6A).

Diazepam, promethazine and propranolol showed a higher binding response value than QN, which was the lowest binding response compound among the effective anti-prion compounds examined in this study. Among these, promethazine or propranolol inhibited PrPres formation in ScNB cells (propranolol: IC_{50}=0.7 μM; promethazine: IC_{50}<5.0 μM). Promethazine has already been reported to have anti-prion activity in ScNB cells,[8] whereas propranolol is a novel compound that inhibits PrPres formation in ScNB cells. Diazepam apparently did not inhibit PrPres formation within a non-toxic dose range up to 25 μM (Fig. 6B). Inhibitory activities against PrPres formation in ScNB cells were not observed for other drugs that had lower binding response values than QN.

DISCUSSION

We demonstrated that most anti-prion compounds examined in this study interacted with PrP121—231. The binding response of the compounds correlated with the IC_{50} of PrPres formation inhibition in ScNB cells. In addition, based on this finding, we proved that this interaction analysis using the SPR method was useful for screening to identify new candidates of anti-prion compounds. Three different *in vitro*

screening assays have been reported recently. One is yeast based,[27] one uses ScN2a cells,[10] and the other is based on fluorescence correlation spectroscopy.[28] These assays are suitable for high-throughput screening of large compound libraries to identify novel lead molecules. The SPR method reported here, which easily assayed interactions between compounds and PrP molecules within less than 3 min per compound, is applicable to high-throughput *in vitro* assay for screening of large compound libraries if more highly performing SPR machines are used. The usefulness of this method in screening for PrP binding ligands is also reported very recently by other researchers.[29]

Two chemicals, ThT and diazepam, showed high binding response but did not inhibit PrPres formation within a non-toxic dose range. Of them, ThT exhibited very low or no affinity with PrP121—231 but the next highest binding response to QC. This suggests that ThT might interact with PrP121—231 non-specifically. For diazepam, similar non-specific interaction with PrP121—231 might be occurred, or the interaction might be specific but unrelated to conversion to PrPres. These inferences, however, remain unsupported by other experimental results obtained here.

On the other hand, such high-affinity compounds as CR and PcTS showed large amounts of binding to PrP121—231. One possible interpretation for this is that the compounds might have two or more binding sites per molecule. In fact, structure–activity relationship analysis for these symmetrical compounds indicates that either half of the molecule has anti-prion activity (Doh-ura K, unpublished data), and their sensorgrams looked very similar to those of anti-PrP antibodies (data not shown). The other is that the compounds might self-assemble to interact with the PrP molecule. It has long been known that CR and many other bis-azo dyes self-assemble in water solutions, and this property is proposed to associate with binding capability.[30]

Instead of the full length of mouse PrP, a carboxy-terminal domain of mouse PrP (PrP121—231) was used in the study because of instability of the full length PrP during the experiment. This carboxy-terminal domain is the only autonomous folding unit of PrP with a defined three-dimensional structure[19,23,24] and contains epitopes recognized by a majority of antibodies bearing anti-prion activity.[31—37] Taken together with our findings suggesting that most of anti-prion compounds might exert their effects by interacting with this domain, targeting the carboxy-terminal domain should not necessarily be either inefficient or inappropriate for looking for new anti-prion compounds.

In conclusion, our study indicated that most anti-prion compounds tested here interacted with and had an affinity for recombinant PrP121—231. The SPR binding response to the PrP121—231 correlated with the anti-prion activity in ScNB cells. These observations will allow further discovery of new classes of anti-prion compounds using the SPR assay.

Acknowledgements This study was supported by grants to K.D. from the Ministry of Health, Labour and Welfare (H16-kokoro-024) and the Ministry of Education, Culture, Sports, Science and Technology (14021085), Japan. The authors thank Dr. Kenta Teruya for critical review of the manuscript.

REFERENCES

1) Prusiner S. B., *Science*, **252**, 1515—1522 (1991).
2) Will R. G., Ironside J. W., Zeidler M., Cousens S. N., Estibeiro K., Alperovitch A., Poser S., Pocchiari M., Smith P. G., *Lancet*, **347**, 921—925 (1996).
3) Brown P., Preece M., Brandel J. P., Sato T., McShane L., Zerr I., Fletcher A., Will R. G., Pocchiari M., Cashman N. R., d'Aignaux J. H., Cervenakova L., Fradkin J., Schonberger L. B., Collins S. J., *Neurology*, **55**, 1075—1081 (2000).
4) Caughey B., Race R. E., *J. Neurochem.*, **59**, 768—771 (1992).
5) Demaimay R., Chesebro B., Caughey B., *Arch. Virol. Suppl.*, **16**, 277—283 (2000).
6) Rudyk H., Vasiljevic S., Hennion R. M., Birkett C. R., Hope J., Gilbert I. H., *J. Gen. Virol.*, **81**, 1155—1164 (2000).
7) Doh-ura K., Iwaki T., Caughey B., *J. Virol.*, **74**, 4894—4897 (2000).
8) Korth C., May B. C., Cohen F. E., Prusiner S. B., *Proc. Natl. Acad. Sci. U.S.A.*, **98**, 9836—9841 (2001).
9) Ryou C., Legname G., Peretz D., Craig J. C., Baldwin M. A., Prusiner S. B., *Lab. Invest.*, **83**, 837—843 (2003).
10) Kocisko D. A., Baron G. S., Rubenstein R., Chen J., Kuizon S., Caughey B., *J. Virol.*, **77**, 10288—10294 (2003).
11) Murakami-Kubo I., Doh-ura K., Ishikawa K., Kawatake S., Sasaki K., Kira J., Ohta S., Iwaki T., *J. Virol.*, **78**, 1281—1288 (2004).
12) Ishikawa K., Doh-ura K., Kudo Y., Nishida N., Murakami-Kubo I., Ando Y., Sawada T., Iwaki T., *J. Gen. Virol.*, **85**, 1785—1790 (2004).
13) Poli G., Martino P. A., Villa S., Carcassola G., Giannino M. L., Dal-l'Ara P., Pollera C., Iussich S., Tranquillo V. M., Bareggi S., Mantegazza P., Ponti W., *Arzneim-Forsch.*, **54**, 406—415 (2004).
14) Sellarajah S., Lekishvili T., Bowring C., Thompsett A. R., Rudyk H., Birkett C. R., Brown D. R., Gilbert I. H., *J. Med. Chem.*, **47**, 5515—5534 (2004).
15) Caughey B., Brown K., Raymond G. J., Katzenstein G. E., Thresher W., *J. Virol.*, **68**, 2135—2141 (1994).
16) Vogtherr M., Grimme S., Elshorst B., Jacobs D. M., Fiebig K., Griesinger C., Zahn R., *J. Med. Chem.*, **46**, 3563—3564 (2003).
17) Caughey W. S., Raymond L. D., Horiuchi M., Caughey B., *Proc. Natl. Acad. Sci. U.S.A.*, **95**, 12117—12122 (1998).
18) Forloni G., Iussich S., Awan T., Colombo L., Angeretti N., Girola L., Bertani I., Poli G., Caramelli M., Grazia Bruzzone M., Farina L., Limido L., Rossi G., Giaccone G., Ironside J. W., Bugiani O., Salmona M., Tagliavini F., *Proc. Natl. Acad. Sci. U.S.A.*, **99**, 10849—10854 (2002).
19) Hornemann S., Glockshuber R., *J. Mol. Biol.*, **261**, 614—619 (1996).
20) Liemann S., Glockshuber R., *Biochemistry*, **38**, 3258—3267 (1999).
21) Johnsson B., Lofas S., Lindquist G., *Anal. Biochem.*, **198**, 268—277 (1991).
22) Myszka D. G., *J. Mol. Recognit.*, **12**, 279—284 (1999).
23) Hornemann S., Korth C., Oesch B., Riek R., Wider G., Wuthrich K., Glockshuber R., *FEBS Lett.*, **413**, 277—281 (1997).
24) Riek R., Hornemann S., Wider G., Billeter M., Glockshuber R., Wuthrich K., *Nature* (London), **382**, 180—182 (1996).
25) Frostell-Karlsson A., Remaeus A., Roos H., Andersson K., Borg P., Hamalainen M., Karlsson R., *J. Med. Chem.*, **43**, 1986—1992 (2000).
26) Tagliavini F., Forloni G., Colombo L., Rossi G., Girola L., Canciani B., Angeretti N., Giampaolo L., Peressini E., Awan T., De Gioia L., Ragg E., Bugiani O., Salmona M., *J. Mol. Biol.*, **300**, 1309—1322 (2000).
27) Bach S., Talarek N., Andrieu T., Vierfond J. M., Mettey Y., Galons H., Dormont D., Meijer L., Cullin C., Blondel M., *Nat. Biotechnol.*, **21**, 1075—1081 (2003).
28) Bertsch U., Winklhofer K. F., Hirschberger T., Bieschke J., Weber P., Hartl F. U., Tavan P., Tatzelt J., Kretzschmar H. A., Giese A., *J. Virol.*, **79**, 7785—7791 (2005).
29) Touil F., Pratt S., Mutter R., Chen B., *J. Pharm. Biomed. Anal.*, **40**, 822—832 (2006).
30) Skowronek M., Roterman I., Konieczny L., Stopa B., Rybarska J., Piekarska B., *J. Comput. Chem.*, **21**, 656—667 (2000).
31) Horiuchi M., Caughey B., *EMBO J.*, **18**, 3193—3203 (1999).
32) Heppner F. L., Musahl C., Arrighi I., Klein M. A., Rulicke T., Oesch B., Zinkernagel R. M., Kalinke U., Aguzzi A., *Science*, **294**, 178—182 (2001).
33) Enari M., Flechsig E., Weissmann C., *Proc. Natl. Acad. Sci. U.S.A.*, **98**, 9295—9299 (2001).

34) Peretz D., Williamson R. A., Kaneko K., Vergara J., Leclerc E., Schmitt-Ulms G., Mehlhorn I. R., Legname G., Wormald M. R., Rudd P. M., Dwek R. A., Burton D. R., Prusiner S. B., *Nature* (London), **412**, 739—743 (2001).
35) White A. R., Enever P., Tayebi M., Mushens R., Linehan J., Brandner S., Anstee D., Collinge J., Hawke S., *Nature* (London), **422**, 80—83 (2003).
36) Féraudet C., Morel N., Simon S., Volland H., Frobert Y., Créminon C., Vilette D., Lehmann S., Grassi J., *J. Biol. Chem.*, **280**, 11247—11258 (2005).
37) Miyamoto K., Nakamura N., Aosasa M., Nishida N., Yokoyama T., Horiuchi H., Furusawa S., Matsuda H., *Biochem. Biophys. Res. Commun.*, **335**, 197—204 (2005).

Available online at www.sciencedirect.com
SCIENCE DIRECT®
Vaccine 24 (2006) 2815–2823
Vaccine
www.elsevier.com/locate/vaccine

Enhanced mucosal immunogenicity of prion protein following fusion with B subunit of *Escherichia coli* heat-labile enterotoxin

Hitoki Yamanaka[a], Daisuke Ishibashi[a], Naohiro Yamaguchi[b], Daisuke Yoshikawa[b], Risa Nakamura[b], Nobuhiko Okimura[b], Takeshi Arakawa[c], Takao Tsuji[d], Shigeru Katamine[b], Suehiro Sakaguchi[a,b,*]

[a] *PRESTO Japan Science and Technology Agency, 4-1-8 Honcho Kawaguchi, Saitama, Japan*
[b] *Department of Molecular Microbiology and Immunology, Nagasaki University Graduate School of Biomedical Sciences, 1-12-4 Sakamoto, Nagasaki 852-8523, Japan*
[c] *Division of Molecular Microbiology, Center of Molecular Biosciences, University of the Ryukyus, 1 Senbaru, Nishihara, Okinawa 903-0213, Japan*
[d] *Department of Microbiology, Fujita Health University School of Medicine, Toyoake, Aichi 470-1192, Japan*

Received 12 May 2005; received in revised form 10 December 2005; accepted 27 December 2005
Available online 17 January 2006

Abstract

Mucosal vaccine against prion protein (PrP), a major component of prions, is urgently awaited since the oral transmission of prions from cattle to humans is highly suspected. In the present study, we produced recombinant bovine and mouse PrPs fused with or without the B subunit of *Escherichia coli* heat-labile enterotoxin (LTB) and intranasally immunized mice with these fused proteins. Fusion with LTB markedly enhanced the mucosal immunogenicity of bovine PrP, producing a marked increase in specific IgG and IgA titer in serum. Mouse PrP also showed slightly increased immunogenicity following fusion with LTB. These results demonstrate that LTB-fused PrPs might be potential candidates for protective mucosal prion vaccines.

Keywords: Prion; Mucosal vaccine; Heat-labile enterotoxin

1. Introduction

Prion diseases including Creutzfeldt-Jakob disease (CJD) in humans, bovine spongiform encephalopathy (BSE) in cattle and scrapie in sheep are devastating neurodegenerative disorders [1,2]. Most cases of CJD are sporadic with unknown etiologies [3]. About 10% of CJD cases are inherited diseases associated with mutations of the prion protein (PrP) gene [3], and most of the remaining cases were iatrogenically transmitted via prion-contaminated electroencephalogram electrodes, human growth hormone preparations, dura matter and corneal grafts [4–7]. Recent lines of evidence indicate that BSE prions could be orally transmitted to humans via contaminated food, causing more than 100 cases of a new variant (nv) CJD in young people, especially in England [8,9]. It is therefore of great importance to develop prion vaccines, in particular those enhancing mucosal immunity, to prevent oral transmission of prions, such as from cattle to humans.

Prions are thought to be mainly composed of the proteinase K (PK)-resistant, amyloidgenic isoform of PrP, designated PrP^{Sc} [10]. PrP^{Sc} is generated by the conformational conversion of the normal isoform of PrP, PrP^{C}, a glycosylphosphatidylinositol-anchored membrane glycoprotein abundantly expressed in neurons [10]. Gabizon et al.

* Corresponding author at: Department of Molecular Microbiology and Immunology, Nagasaki University Graduate School of Biomedical Sciences, 1-12-4 Sakamoto, Nagasaki 852-8523, Japan. Tel.: +81 95 849 7059; fax: +81 95 849 7060.
E-mail address: suehiros-ngs@umin.ac.jp (S. Sakaguchi).

0264-410X/$ – see front matter © 2006 Elsevier Ltd. All rights reserved.
doi:10.1016/j.vaccine.2005.12.054

previously reported that polyclonal antibodies against PrP could reduce the infectivity of hamster-adapted scrapie prions [11]. Heppner et al. also recently showed that mice transgenically expressing anti-PrP monoclonal antibody, 6H4, were resistant to the disease after intraperitoneal inoculation of mouse-adapted scrapie RML prions [12]. It was further reported that passive immunization with two other anti-PrP monoclonal antibodies, ICSM 18 and 35, could protect mice from prion infection [13]. Such successful prevention of the prion infection by anti-PrP antibodies indicates that mucosal vaccination against PrP could be a more rational way to block the oral transmission of prions. However, the host is already immunologically tolerant to PrP, hampering the development of prion vaccines.

Escherichia coli heat-labile enterotoxin (LT) and cholera toxin (CT) are highly potent adjuvants for mucosal immunity [14,15]. The mechanism of how these toxins elicit mucosal immunity is not fully understood. These toxins consist of one A subunit and a pentamer of B subunits [14,15]. The A subunit carries enzymatic activity and the B subunit pentamer mediates binding of the toxins to GM_1 gangliosides on target epithelial cells [14,15]. Upon binding of these toxins to cells, the A subunit enters the cells and exerts its toxicity via ADP-ribosylation of adenylate cyclase [14,15]. The B subunit of LT (LTB) or CT (CTB) is a strong modulator of mucosal immunity and fusion with these B subunits could enhance the mucosal immunogenicity of certain peptides [14,15].

In the present study, we successfully demonstrate for the first time that fusion with LTB markedly enhanced the mucosal immunogenicity of bovine (bo) PrP to elicit strong antibody responses in mice. Slightly increased responses could also be observed against mouse (mo) PrP fused with LTB in mice.

2. Materials and methods

2.1. Plasmid construction and purification of recombinant PrPs

2.1.1. LTB-moPrP120-231 and LTB-boPrP132-242

The DNA fragment for LTB residues 22–124 (*E. coli* MV1184) with sequences for the *Eco*RV site at the 5′-terminus and for the Gly-Pro-Gly-Pro and *Eco*RI site at the 3′-terminus was amplified by polymerase chain reaction (PCR). The fragment for moPrP residues 120–231 (GenBank accession no. M13685) and boPrP residues 132–242 (D10612) containing the *Eco*RI site at the 5′-terminus and the *Xho*I site at the 3′-terminus, were similarly amplified by PCR. Following sequence confirmation of these PCR products, the LTB and PrP fragments were digested and simultaneously inserted into a pET20b(+) vector (Novagen Inc., WI, USA), resulting in pET-LTB-moPrP120–231 and pET-LTB-boPrP132–242. *E. coli* (BL21) cells being transformed by these plasmids and cultured in LB medium. The recombinant proteins were expressed by 1 mM isopropyl β-D-thiogalactoside (IPTG). The cells were collected by centrifugation, lysed using CelLytic B Bacterial Cell Lysis/Extraction Reagent (Sigma–Aldrich Co., St Louis, USA) in the presence of DNase I, and centrifuged at 25,000 × *g* for 10 min. The resulting supernatant was purified using a Ni-NTA column (Qiagen, Hilden, Germany) under native conditions as recommended in the manufacturer's protocol.

2.1.2. moPrP120–231 and boPrP132–242

The DNA fragments encompassing moPrP residues 120–231 and boPrP residues 132–242 were amplified by PCR. The *Bam*HI and *Hin*dIII sites were introduced at the 5′- and 3′-termini of these fragments, respectively. These fragments were then digested and inserted into a pQE30 vector (Qiagen), resulting in pQE30-moPrP120–231 and pQE30-boPrP132–242. *E. coli* (M15) cells were transformed by these plasmids and cultured in LB medium containing 1 mM IPTG. The cells were collected by centrifugation, suspended in PBS containing 2% Triton X-100, and lysed by ultrasonication. This lysate was centrifuged at 35,000 × *g* for 15 min. The resulting pellet was resolved in PBS containing 8 M urea and 20 mM 2-mercaptoethanol and applied to a Ni-NTA column (Qiagen). The proteins were finally eluted with PBS containing 500 mM imidazole.

2.1.3. moPrP23–231 without a 6 × His tag

The DNA fragment for moPrP residues 23–231 with the *Nde*I site at the 5′-terminus and the *Bam*HI site at the 3′-terminus were amplified by PCR. The fragment was digested and inserted into pET11a (Novagen), resulting in pET11a-moPrP23–231. *E. coli* (BL21) cells were transformed with the plasmid and cultured in LB medium containing 1 mM IPTG. The cells were collected by centrifugation and resuspended in a buffer (50 mM Tris–HCl, pH 8, 1 mM EDTA, 100 mM NaCl, 1 mM PMSF) containing 300 μg/ml lysozyme, deoxycholic acid and DNase I. The resulting extract was centrifuged at 25,000 × *g* for 20 min and the pellet was solubilized in a buffer (8 M urea, 50 mM Tris–HCl, 1 mM EDTA, pH 8). This extract was applied to a CM-sepharose column (Amersham Pharmacia Biotech AB, Uppsala, Sweden) and recombinant PrP was eluted using a linear NaCl gradient from 0 to 500 mM.

2.2. GM_1 ganglioside binding assay

A 96 well immunoplate (Nunc, Roskilde, Denmark) was coated with 200 ng of GM_1 ganglioside (Sigma–Aldrich Co.) in a 50 mM carbonate buffer (pH 9.6) and blocked with PBS containing 0.05% Tween-20 and 25% Block Ace (Dainihonseiyaku Co., Tokyo, Japan). The fusion proteins were incubated in the wells for 1 h at 37 °C. Binding of the proteins to GM_1 ganglioside was visualized using anti-LT mouse serum raised against recombinant LT and anti-mouse IgG antibodies conjugated with horseradish peroxidase (HRP, Amersham Biosciences, NJ, USA).

2.3. Nasal immunization of mice with PrPs

Purified proteins were dialyzed against PBS and 10 μl containing 10 μg proteins and 1 μg of an adjuvant mutant LT were administered into each external nare of female 8-week-old C57BL/6 and Balb/c mice (SLC Japan, Shizuoka, Japan) at 2-week intervals. Mutant LT toxin lacking residues Arg192, Thr193 and Ile194 in the A subunit was prepared as previously described [16]. Mice were cared for in accordance with the Guidelines for Animal Experimentation of Nagasaki University.

2.4. Determination of specific IgG and IgA antibody titers

Each well of a 96 well immunoplate (Nunc) was coated with 500 ng of purified moPrP without a 6 × His tag or 6 × His-tagged boPrP by overnight incubation at 4 °C and then blocked with PBS containing 0.05% Tween-20 (T-PBS) and 25% Block Ace (Dainihonseiyaku Co.) at 37 °C for 1 h. To detect anti-boPrP or anti-moPrP antibodies, serially 10- or 8-fold diluted antiserum was added to the wells for 1 h at 37 °C, respectively, and unbound antibodies were removed by washing twice with T-PBS. Immune complexes were detected using secondary goat anti-mouse IgA (Sigma) or sheep anti-mouse IgG antibodies conjugated with HRP (Amersham Biosciences).

2.5. Quantification of anti-PrP IgA in fecal extract

Each well of a 96 well immunoplate (Nunc) was coated with 500 ng of purified 6 × His-tagged boPrP by overnight incubation at 4 °C and then blocked with PBS containing 0.05% Tween-20 (T-PBS) and 25% Block Ace (Dainihonseiyaku Co.) at RT for 1 h. The fecal extracts were prepared according to a manufacturer's protocol. In brief, ~30 mg of feces were homogenized in 600 μl of PBS containing a protease inhibitor cocktail (Nacalai Tesque Inc., Kyoto, Japan) and centrifuged to remove insoluble materials. Two-fold diluted supernatant of the fecal extract was added to the wells for 1 h at RT and unbound antibodies were removed by washing twice with T-PBS. Immune complexes were detected using secondary goat anti-mouse IgA antibody conjugated with HRP (Amersham Biosciences). The concentration of specific IgA in the fecal extract was determined from a standard curve plotted using an already-known standard concentration of IgA (BETHYL Lab. Inc., Texas, USA).

2.6. Transfection

African green monkey kidney COS-7 cells were cultured in Dulbecco's modified Eagle medium (Invitrogen, Carlsbad, CA) containing 10% fetal bovine serum and transfected by a pcDNA3.1 vector (Invitrogen) inserted with or without the cDNA encoding bo, sheep (sh), and human (hu) PrP^C using lipofectamin 2000 (Invitrogen). These cells were then subjected to immunoblotting or FACS analysis 3 days after transfection.

2.7. Immunoblotting

COS-7 cells were lysed in buffer (1% Triton X-100, 1% sodium deoxycholate, 300 mM NaCl, 100 mM Tris–HCl, pH 7.5) and brain tissues were homogenized in PBS. Thirty micrograms of total proteins were treated with or without 20 μg/ml proteinase K for 30 min at 37 °C, electrophoresed on a 12% SDS-polyacrylamide gel, and electrically transferred onto a nitrocellulose membrane (Millipore, MA, USA). The membrane was incubated with antiserum for 2 h. The signals were visualized using HRP-conjugated secondary anti-mouse IgG antibodies and the ECL system (Amersham Biosciences).

2.8. FACS

Cells were harvested with PBS containing 0.2% EDTA, suspended in BSS buffer (140 mM NaCl, 5.4 mM KCl, 0.8 mM $MgSO_4$, 0.3 mM Na_2HPO_4, 0.4 mM KH_2PO_4, 1 mM $CaCl_2$), and incubated with 100-fold diluted antisera for 30 min on ice. The treated cells were then washed three times with BSS buffer, reacted with FITC-conjugated goat anti-mouse IgG (H + L) (Chemicon International, CA, USA), and analyzed by FACScan (Becton Dickinson, New Jersey, USA).

3. Results

3.1. Purification and characterization of LTB-fused mo and boPrPs

Since the C-terminal half of moPrP was shown to be recombinantly expressed in large amounts of soluble protein in the periplasmic space of *E. coli.* [17] and include the epitopes for anti-mouse prion antibodies [12,13], we constructed LTB-moPrP120–231 fusion protein by linking the C-terminal residues 120–231 of moPrP to the C-terminus of LTB with the hinge sequence Gly-Pro-Gly-Pro (Fig. 1a). LTB-boPrP132–242 was similarly constructed by fusion of boPrP residues 132–242 with LTB (Fig. 1a). These fusion proteins contain the signal peptide at the N-terminus to be secreted into the periplasmic space and a 6 × His sequence at the C-terminus allowing easy purification using a Ni-NTA column.

We partially purified these recombinant proteins in a soluble form. Coomassie brilliant blue staining of denatured LTB-moPrP120–231 and LTB-boPrP132–242 showed one major band with a molecular weight of ~25 kDa, corresponding to the monomeric fusion protein (Fig. 1b). In contrast, under non-denaturing electrophoresis conditions, these bands disappeared and were shifted to higher molecular weight ladder bands including one major band (Fig. 1b). The molecular

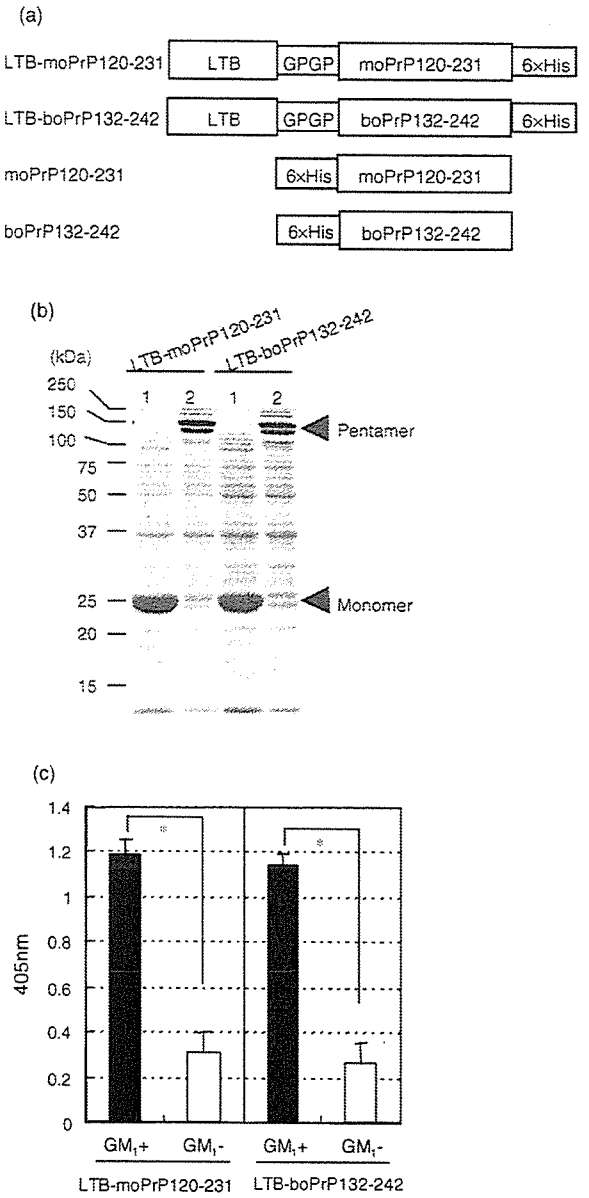

Fig. 1. Structural diagrams of mouse (mo) and bovine (bo) PrPs fused with or without LTB (a) and biochemical properties of LTB-fused PrPs (b and c). (b) LTB-moPrP120–231 and LTB-boPrP132–242 were boiled at 100 °C in denatured conditions and then electrophoresed on a 12% SDS-PAGE (lane no. 1). These denatured fusion proteins were monomeric. In contrast, without boiling (lane no. 2), the fusion proteins formed a pentameric structure. (c) LTB-moPrP120–231 and LTB-boPrP132–242 similarly bound to GM_1 ganglioside. The signals were expressed as colorimetric values measured at 405 nm. Four independent data from each group were analyzed using the Mann–Whitney *U*-test. Data were represented by mean ± standard deviation (S.D.). $^{*}p<0.05$.

weight of these bands indicates that fusion proteins are at least pentameric in a native form.

We also examined whether these fusion proteins could bind to GM_1 ganglioside. The fusion proteins were first incubated on plates with or without immobilized GM_1 ganglioside and then colorimetrically detected by anti-LT antibodies. The colorimetric values obtained from complexes of fusion proteins bound to GM_1 ganglioside were significantly much higher than those of the fusion protein alone (Fig. 1c). Anti-PrP polyclonal antibodies also showed similar binding of the fusion proteins to GM_1 ganglioside (data not shown). These results thus indicate that the fusion proteins have conserved binding competence to GM_1 ganglioside.

3.2. Enhancement of mucosal immunogenicity of boPrP132–242 by fusion to LTB

To examine the effect of fusion with LTB on the mucosal immunogenicity of boPrP132–242, we intranasally immunized C57BL/6 and Balb/c mice with LTB-boPrP132–242 as well as non-fused boPrP132–242 as a control three times at 2-week intervals in the presence of recombinant mutant LT as an adjuvant. BoPrP132–242 was N-terminally tagged with a 6 × His sequence (Fig. 1a) and purified using a Ni-NTA column. Antisera were collected from these mice 1 week after the final immunization and subjected to ELISA against recombinant boPrP with a 6 × His tag to determine specific IgG and IgA antibody titers. BoPrP132–242 itself elicited a moderate IgG antibody response in Balb/c mice but not in C57BL/6 mice (Fig. 2a). No efficient IgA response against boPrP132–242 could be detected in either mouse strain (Fig. 2a). In contrast, LTB-boPrP132–242 markedly enhanced the immunogenicity in both mouse strains, producing an enhanced increase in anti-boPrP IgG and IgA titers in serum, except for IgA in C57BL/6 mice (Fig. 2a). A large amount of specific secretory IgA was consistently detected in the feces of LTB-boPrP132–242-immunized Balb/c mice (Fig. 2b).

3.3. Detection of native PrP^C and PrP^{Sc} by anti-LTB-boPrP132–242 serum

To examine whether the anti-LTB-boPrP132–242 sera could recognize native PrP^C, we first performed Western blotting of the COS-7 cell lysates expressing non-6 × His-tagged bo, sheep (sh), and human (hu) PrP^C with the antisera from the immunized Balb/c mice. No specific signals could be detected in the cells transfected with a control vector (Fig. 3a). $MoPrP^C$ could not be detected with the antisera (data not shown). In contrast, the antisera strongly reacted with bo and $shPrP^C$ and weakly with $huPrP^C$ (Fig. 3a). We next carried out FACS analysis of these cells with the antisera. Vector alone-transfected cells showed no signals (Fig. 3b). In contrast, a large number of the cells expressing bo, sh and $huPrP^C$ could be stained (Fig. 3b). These results indicate that LTB-boPrP132–242 could induce antibodies recognizing native PrP^C from a broad range of species.

We also performed Western blotting of the brains of normal and BSE-affected cattle as well as those of scrapie-affected sheep with the anti-LTB-boPrP132–242 serum. In the normal cattle, specific signals could be detected only in

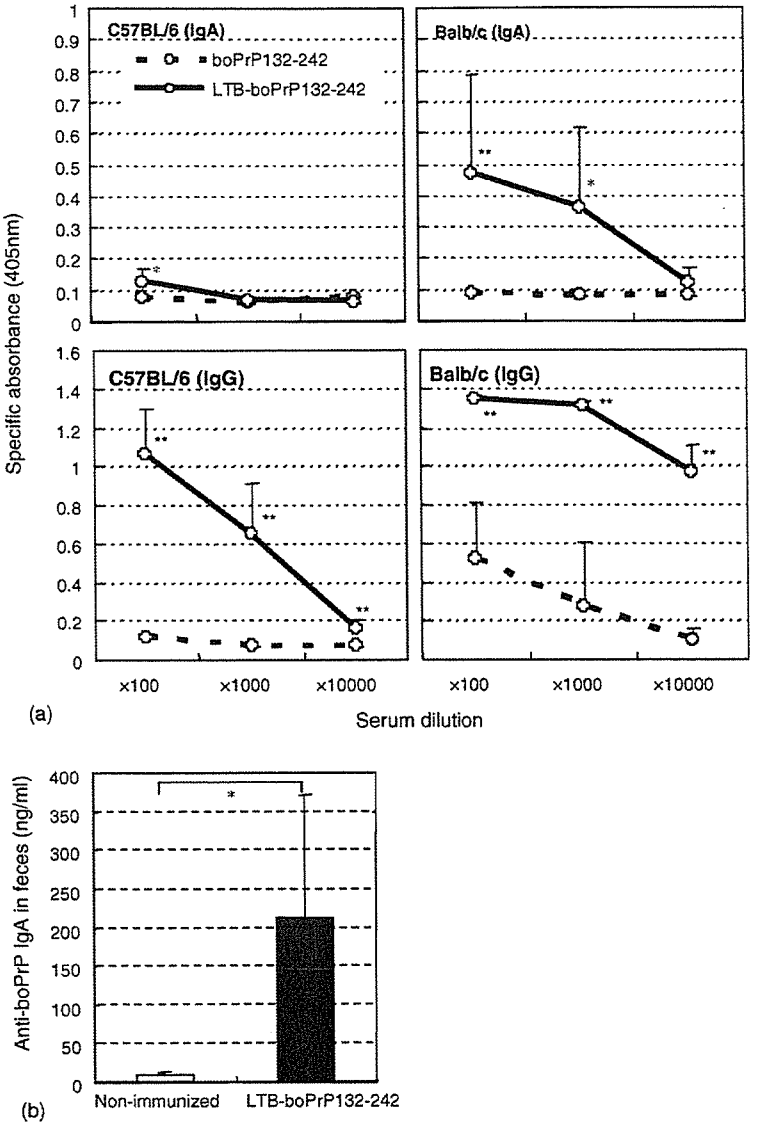

Fig. 2. (a) Specific IgA and IgG antibody titers in the serum of C57Bl/6 and Balb/c mice intranasally immunized with LTB-boPrP132–242 or boPrP132–242 three times at 2-week intervals. Antisera were collected from five mice from each group and were subjected to ELISA against 6 × His-tagged boPrP. Antibody titers were expressed by colorimetric values at 405 nm. (b) Amounts of specific IgA secreted in the feces of mice intranasally immunized with LTB-boPrP132–242 six times at 2-week intervals. Data were analyzed using the Mann–Whitney *U*-test. Data were represented by mean ± S.D. $^{*}p<0.05$; $^{**}p<0.01$.

the samples treated without PK (Fig. 3c), indicating that this antiserum could recognize boPrP^{C} in normal cattle brains. Moreover, this antiserum could detect bo and shPrP^{Sc} accumulated in the brains of BSE-cattle and scrapie-sheep, respectively (Fig. 3c).

3.4. Anti-LTB-boPrP132–242 antibodies recognize a potential anti-BSE prion epitope

Protective monoclonal antibodies, ICSN 35, 6H4 and ICSN 18, were shown to bind to moPrP residues 91–110, 144–152 and 146–159, respectively [12,13]. In addition, R1 and R2 Fab fragments bind to moPrP residues 220–231 and inhibit the accumulation of PrP^{Sc} in mouse neuroblastoma N2a cells infected with a prion [18]. These results strongly suggest that the corresponding regions in other PrPs are also potential anti-prion epitopes. To examine whether the antibodies against LTB-boPrP132–242 could react with these epitopes, we expressed the corresponding regions, boPrP residues 94–121, 143–166 and 231–242, as a fusion protein with glutathione *S*-transferase (GST) and subjected these proteins to Western blotting with the antisera. GST alone and GST-boPrP 94–121 and 231–242 could not be detected with the sera (Fig. 3d). However, GST-boPrP